Gamma-ray astronomy / Astronomie des rayons gamma – Volume 2

Active galactic nuclei at gamma-ray energies

CrossMark

Noyaux actifs de galaxie dans le domaine des rayons gamma

Charles Dennison Dermer [a,*], Berrie Giebels [b]

[a] Code 7653, Naval Research Laboratory, Washington, DC, USA
[b] LLR, École polytechnique, CNRS/IN2P3, Université Paris-Saclay, 91128 Palaiseau cedex, France

A B S T R A C T

Active Galactic Nuclei can be copious extragalactic emitters of MeV–GeV–TeV γ rays, a phenomenon linked to the presence of relativistic jets powered by a super-massive black hole in the center of the host galaxy. Most of γ-ray emitting active galactic nuclei, with more than 1500 known at GeV energies, and more than 60 at TeV energies, are called "blazars". The standard blazar paradigm features a jet of relativistic magnetized plasma ejected from the neighborhood of a spinning and accreting super-massive black hole, close to the observer direction. Two classes of blazars are distinguished from observations: the flat-spectrum radio-quasar class (FSRQ) is characterized by strong external radiation fields, emission of broad optical lines, and dust tori. The BL Lac class (from the name of one of its members, BL Lacertae) corresponds to weaker advection-dominated flows with γ-ray spectra dominated by the inverse Compton effect on synchrotron photons. This paradigm has been very successful for modeling the broadband spectral energy distributions of blazars. However, many fundamental issues remain, including the role of hadronic processes and the rapid variability of a few FSRQs and several BL Lac objects whose synchrotron spectrum peaks at UV or X-ray frequencies. A class of γ-ray-emitting radio galaxies, which are thought to be the misaligned counterparts of blazars, has emerged from the results of the Fermi-Large Area Telescope and of ground-based Cherenkov telescopes. Soft γ-ray emission has been detected from a few nearby Seyfert galaxies, though it is not clear whether those γ rays originate from the nucleus. Blazars and their misaligned counterparts make up most of the $\gtrsim 100$ MeV extragalactic γ-ray background (EGB), and are suspected of being the sources of ultra-high energy cosmic rays. The future "Cherenkov Telescope Array", in synergy with the Fermi-Large Area Telescope and a wide range of telescopes in space and on the ground, will write the next chapter of blazar physics.

© 2016 Académie des sciences. Published by Elsevier Masson SAS. All rights reserved.

R É S U M É

Les noyaux actifs de galaxie peuvent être de puissants émetteurs dans tout le domaine γ, du MeV au TeV, un phénomène dû à la présence de jets relativistes, en liaison avec un trou noir super-massif au centre de la galaxie hôte. La classe d'émetteurs de rayons γ la plus abondante parmi les noyaux actifs de galaxie, avec plus de 1500

* Corresponding author.
  E-mail addresses: charlesdermer@outlook.com (C.D. Dermer), Berrie.Giebels@CNRS.fr (B. Giebels).

sources établies aux énergies du GeV, et plus de 60 aux énergies du TeV, sont les « blazars ». Le paradigme actuel du blazar met en jeu un jet de plasma magnétisé, orienté à faible angle de la ligne de visée, et éjecté depuis le voisinage d'un trou noir accrétant et super-massif en rotation. Les observations permettent de distinguer deux types de blazars : les quasars radio à spectre plat (ou FSRQ) comprennent des champs de rayonnement externes puissants, des zones avec des raies d'émission optiques larges, et des tores de poussières. La classe des BL Lac (du nom d'un de ses membres, BL Lacertae) possède des flots d'accrétion plus faibles, dominés par l'advection, et dans lequel l'émission des rayons γ vient essentiellement de l'effet Compton inverse sur les photons synchrotron. Ce paradigme permet de modéliser l'émission des blazars sur tout le spectre électromagnétique. Cependant, beaucoup de problèmes fondamentaux restent sans réponse, notamment le rôle des processus hadroniques, et la variabilité très rapide de l'émission de certains objets BL Lac, ceux dont le spectre synchrotron émet le maximum de puissance dans les domaines UV et X. Les observations du satellite Fermi-LAT et celles des observatoires Tcherenkov au sol ont également mis en évidence une nouvelle classe de radio-galaxies émettrices de rayons γ, considérées comme les contreparties non alignées des blazars. On a aussi détecté l'émission de rayons γ de basse énergie provenant de galaxies de type Seyfert, mais il n'est pas encore sûr que cette émission vienne du noyau. Les blazars avec leurs contreparties non alignées sont à l'origine de la plus grande partie de l'émission gamma extragalactique diffuse au-dessus de 100 MeV, et sont soupçonnés d'être les sources des rayons cosmiques d'ultra-haute énergie. Le futur réseau *Cherenkov Telescope Array* (CTA), en synergie avec le télescope spatial Fermi et une grande variété de télescopes dans l'espace et au sol, écriront le prochain chapitre de la physique des blazars.

1. Introduction: AGN detected at γ-ray energies

Among the astrophysical γ-ray emitters located well beyond the Milky Way are the γ-ray galaxies. From the recent advances in the field we can classify, simply, two types of γ-ray galaxies. First are the *black-hole galaxies*, which are powered by infalling gas onto a massive black hole in their center, and will be thoroughly discussed here. Second are the generally much weaker and likely more numerous *cosmic-ray galaxies* with their γ-ray emission powered by stellar explosions rather than black holes, which make shocks that accelerate cosmic rays [1]. Indeed, galaxies hardly have to harbor a radio-luminous black hole to be γ-ray luminous, as confirmed by a quick glance at the Fermi-LAT all-sky image, which shows the Milky Way lit up by cosmic rays colliding with diffuse gas and dust. Besides most γ rays produced by nuclear collisions of cosmic rays to make pions, cosmic-ray galaxies are also illuminated in γ rays by pulsars and pulsar-wind nebulae. Analysis shows that black-hole galaxies make the bulk of the high-energy (HE; $\gtrsim$100 MeV) and Very High Energy (VHE; $\gtrsim$100 GeV) extragalactic γ-ray background (EGB, [2]). Cosmic-ray galaxies, because they essentially partake in hadronic processes, should have comparable neutrino and γ-ray luminosities. Note how different these two types of γ-ray galaxies are in comparison with the two types of γ-ray emitting black-hole galaxies, namely Seyferts and blazars, identified in the CGRO days [3].

The black-hole γ-ray galaxies are Active Galactic Nuclei (AGN), which are among the most powerful known astrophysical sources of non-thermal radiation and most luminous known electromagnetic emitters, with luminosities in the range 10^{35}–10^{41} W.

1.1. The active galaxy zoo

The observational classification of AGN, dominated by the dichotomy between radio-quiet and radio-loud classes, with the latter constituting 10% of the population, is represented in the chart of Fig. 1. The less numerous radio-loud AGN are about 3 orders of magnitude brighter in the radio band than their radio-quiet counterparts.

The AGN unification scheme is based on the sketch by Urry and Padovani [4] (see Fig. 2) which displays the composite AGN phenomenon (black hole, disk, torus, clouds and jet), and illustrates how orientation effects, different accretion powers, and different spin parameters[1] a/M of the black hole could account for the wide range of AGN types. According to Fig. 2, the appearance of an AGN depends crucially on the orientation of the observer with respect to the symmetry axis of the accretion disk. In this picture, the difference between radio-loud and radio-quiet AGN depends on the presence or absence of radio-emitting jets powered by the central nucleus, which in turn may be induced by the rotation of the black hole. In Fig. 2, at high accretion rates (relative to the Eddington limit) and large luminosities, both radio-loud and radio-quiet AGN have dusty tori, broad-line regions (BLRs), narrow-line regions, and strong big blue/UV bump emissions from an optically thick accretion disk. BLR clouds illuminated by the accretion-disk radiation are obscured in Seyfert 2 AGN when viewing

---

[1] The spin parameter is the ratio of the angular momentum a of the black hole to its mass M.
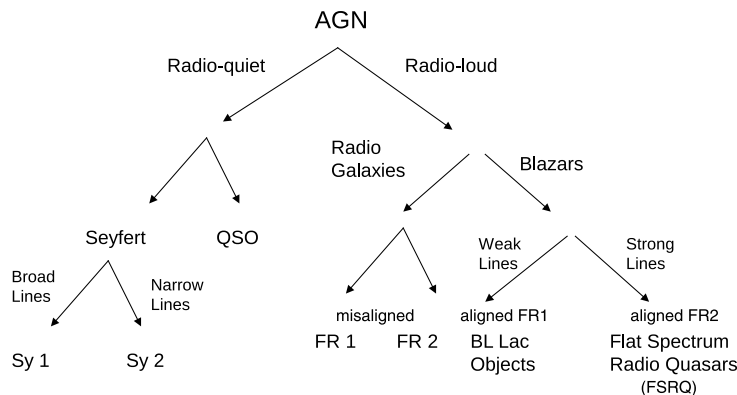
Fig. 1. Observational classification of active galaxies. AGN are subdivided into classes depending on observational aspects, such as their radio loudness or the presence of optical lines in their spectra. QSO = quasi-stellar objects; Sy1 and Sy2 = Seyfert 1 and 2; FR1 and FR2 = Fanaroff–Riley 1 and 2.

through the dusty torus, and so only narrow lines from high-altitude[2] material far from the black hole are seen, resulting in a narrow-line AGN. By comparison, broad lines are seen from Seyfert 1 AGN when viewing at higher latitudes[3] so that the central nucleus and BLR are visible.

When the jet is directed close to the line of sight ("aligned" jet), two AGN subclasses are distinguished from observations:

– BL Lac objects, corresponding to the aligned jets of low-luminosity Fanaroff–Riley 1 (FR1)[4] radio galaxies (but this classification could miss the type of BL Lac objects that arises from the beamed radiation overwhelming the lines and disk radiation).
– Flat Spectrum Radio Quasars (FSRQ, with a radio spectral index $\alpha \sim 0$ at a few GHz), corresponding to the aligned jets of higher luminosity Fanaroff–Riley 2 (FR2) radio galaxies.

As illustrated in Fig. 2, BL Lac objects occur in AGN with no significant accretion disk, broad lines, or dusty torus [6]. In low-luminosity AGN, advective effects in accretion likely play an important role in accounting for the relationship between escaping photon power and accretion power.

Narrow-line and broad-line radio galaxies likewise depend on the direction of the observer's line of sight with respect to the angle of the disk-jet system, and would more likely be associated with FR2 radio galaxies. Blazars are those sources for which we happen to be viewing at an angle $\theta \lesssim 1/\Gamma$, that is, within the Doppler beaming cone of the relativistically outflowing plasma moving with bulk Lorentz factor Γ. The powerful FSRQs also have strong broad optical lines, indicating the presence of accretion-disk radiation and dense broad-line region material. The low-luminosity counterparts of the radio-loud AGN are the BL Lac objects and their misaligned counterparts, the FR1 radio galaxies. Since blazars are relativistically beamed and aligned objects, their misaligned counterparts should be more numerous, but the interpretation of the measured source counts of the two classes must take into account beaming corrections.

1.2. History of active galactic research at gamma-ray energies

The growth and development of space-based γ-ray astronomy (see [8] in the first volume of this review) owes much to the pioneering missions OSO-3 (1967–1968), SAS-2 (1972–1973) and COS-B (1975–1982) [9], but the γ-ray astronomy of active galactic nuclei (AGN) cannot be said to have begun until the launch of the *Compton* Gamma Ray Observatory (CGRO) in 1991. Prior to the EGRET (Energetic Gamma ray Experiment Telescope) on CGRO [10], five γ-ray emitting AGN were known, but what a mixed bag! As reviewed by Bassani and Dean [11], these included the Seyfert galaxies NGC 4151 and MCG 6-11-11, the radio galaxy Centaurus A, the "peculiar galaxy" NGC 1275, and the quasar 3C 273. Only 3C 273 was detected at $\gtrsim 35$ MeV energies—by COS-B—whereas the others had emission extending only to a few hundred keV.

The first EGRET pointing towards 3C 273 revealed a bright flaring source, but at the position of the quasar 3C 279. By the end of the first year of the mission, more than 14 γ-ray emitting AGN between ~ 100 MeV and 5 GeV were found. Most detections were prominent radio-loud quasars, including PKS 0528+134, 3C 454.3, and CTA 102, but they also included the BL Lac object Mrk 421. The strong connection with apparently superluminal[5] radio sources implied that the γ rays come

---

[2] The altitude is the distance to the central nucleus projected along the rotation axis of the accretion-disk/torus system.

[3] Similarly, the latitude is defined as the angle with respect to the accretion disk considered as an equatorial plane.

[4] According to the Fanaroff–Riley classification [5], FR1 have radio jets that are brighter in the center, while FR2 object jets are fainter towards the center but feature brighter radio spots towards the end of their jets.

[5] When the radiative zone is moving at relativistic velocity along a direction close to the line of sight, its apparent velocity as measured on the basis of the observer's proper time may be greater than c.
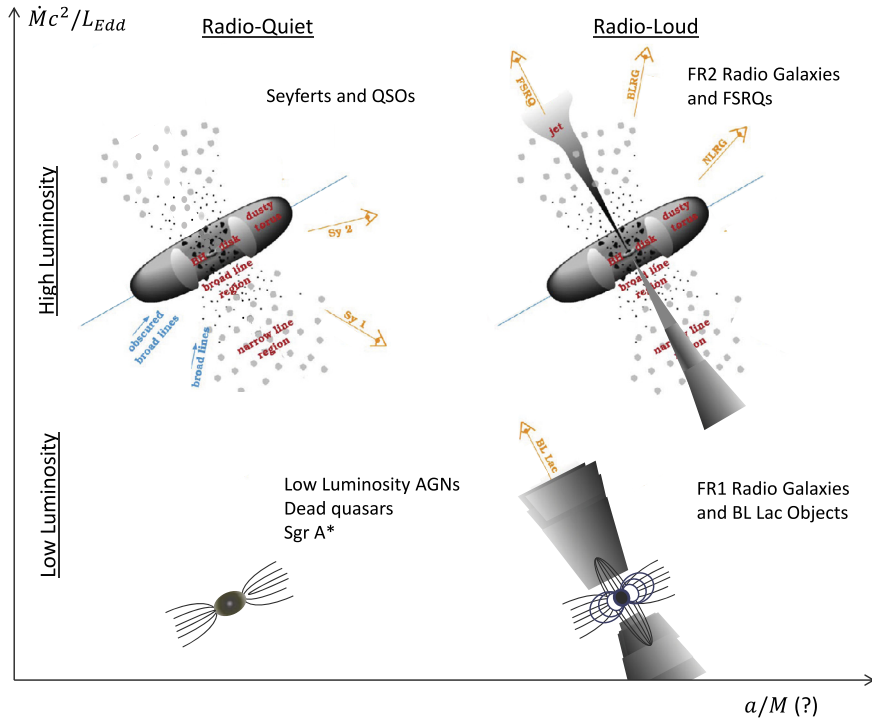
Fig. 2. Types of active galaxies. Cartoon illustration of AGN taxonomy, following the unification scheme for radio-quiet and radio-loud galaxies, *cf.* [7] as adapted from [4]. In this two-parameter model, including orientation, any given AGN is either radio-quiet or radio-loud, here speculated to depend on black-hole rotation a/M (where M is the black hole mass, and a its angular momentum), or low power or high power, as determined by the mass-accretion rate. The misaligned AGN sources are the radio galaxies, including the low luminosity FR1 counterparts to BL Lac objects, and high luminosity FR2 radio galaxies, which divide into narrow- and broad-line radio galaxies, depending on orientation.

from a nearly aligned relativistic jet of a black hole [12], and the γ-ray blazar class emerged. By the end of the CGRO mission, 66 high-confidence and 27 low-confidence detections of blazars had been made, including the radio galaxy Cen A [13]; see Fig. 3 left.

During the same time, a major advance in ground-based γ-ray astronomy took place when the on-off approach was superseded by the imaging Atmospheric Cherenkov Technique (ACT) [14], leading to the significant detection of the Crab nebula at Very High Energies (VHE; $\gtrsim$100 GeV) with the pioneering Whipple array [15]. Soon after the recognition that blazars are EGRET sources, Mrk 421 was found to be a VHE source [16]. The VHE discovery of Mrk 501 was reported in 1995, and the pace of discovery has since quickened, particularly with the introduction of new detectors and arrays. The largest class of VHE AGN sources consists of BL Lac objects, which all show a characteristic double-humped spectral energy distribution (SED) in νF_ν representation[6]; this structure will be further described and interpreted in the following sections. For most of them, the low-energy peak is typically located in the UV and X-ray ranges ($\nu_s > 10^{15}$ Hz). Soon however radio galaxies (e.g., M87), low-peaked BL Lac objects like AP Lib and BL Lac itself, and even FSRQs have been detected at VHE; see Fig. 3 right.

Extragalactic γ-ray emitters now constitute more than half of the high-energy (HE; $E > 100$ MeV) emitters identified by the Large Area Telescope (LAT) on the Fermi Gamma ray Space Telescope [10], and are the second largest population, after pulsar-wind nebulae, in the ground-based VHE regime.[7] Although radio-loud AGN represent only $\sim$10% of all AGN, the overwhelming majority of known extragalactic γ-ray sources are radio-loud AGN, where some physical process "turns on" the supermassive black hole to make a radio jet. Much speculation has focused on tapping the energy of rotation through processes occurring in the spinning black hole's magnetosphere. Plasma processes in the jet activate a particle acceleration mechanism whose details still elude us, though shock acceleration and magnetic reconnection are plausible mechanisms. The interaction of the energetic particles (whether leptonic or hadronic) with ambient radiation or magnetic fields then generate, through well-known relativistic radiation physics [23], the copious amounts of γ rays that are often observed from γ-ray blazars, including extreme states with rapid flux variations, large apparent luminosities, and HE and VHE γ-ray photons escaping from very compact volumes.

---

[6] For the definition and the interest of the SED, see [8]; ν is the frequency and F_ν is the power received per unit area and frequency.

[7] According to TeVCat; see http://tevcat.uchicago.edu.
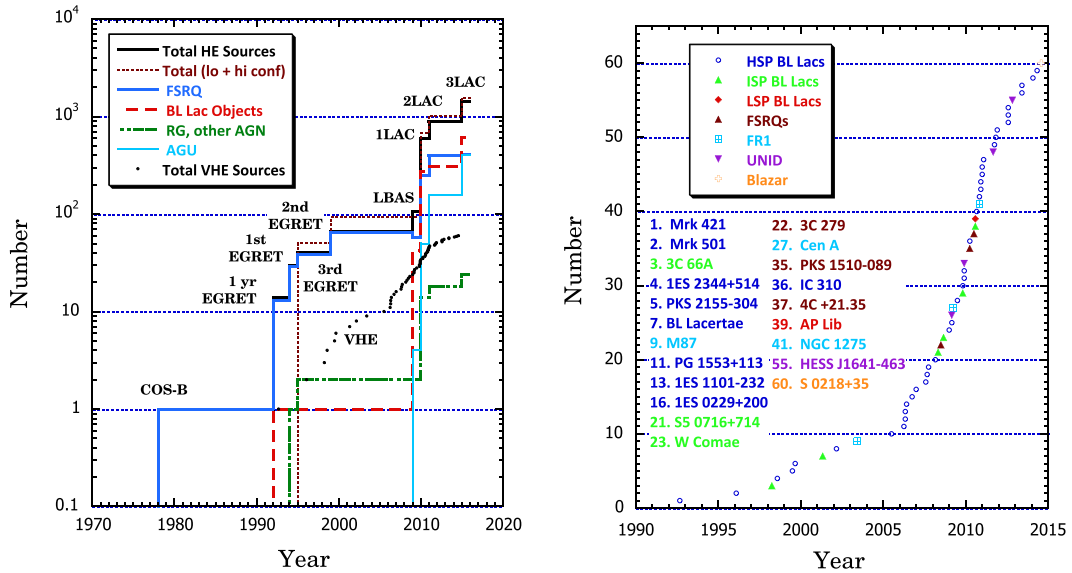
Fig. 3. The growth rate of γ-ray AGN at GeV and TeV energies. *(a; left)* Growth of sources at high-energy (HE), $\gtrsim 100$ MeV, γ rays. The number of sources reported in the different catalogs and lists, as noted in the figure, are from the 1st EGRET Catalog [17]; 2nd EGRET Catalog [18]; 3rd EGRET catalog [13]; LAT Bright AGN Sample (LBAS) [19], First LAT AGN Catalog (1LAC) [20], 2LAC [21], and the 3LAC [22]. *(b; right)* Number of VHE AGN detected by Atmospheric Cherenkov Detectors (ACTs), obtained using the TeVCat. While the brightest and nearest AGN have been detected by the previous generation of ACTs such as the Whipple observatory, HEGRA, and CAT, a clear break in the discovery rate occurs after 2004 when the new generation of instruments started observing. While the bulk of extragalactic VHE sources are BL Lac type blazars (such as Mrk421, the first discovered of that type), a few radio-galaxies (M87, Cen A, and NGC 1275) and FSRQ-type blazars (3C279, PKS 1510-89, and 4C +21.35) are now also significantly detected. See section 2.1 for the definition of other acronyms used in these figures.

2. Classification of AGN detected in γ rays

Back in 1983, when extragalactic γ-ray astronomy was in its infancy with a handful of sources, early classification attempts were made by e.g. Bassani & Dean [11]. The listed sources were divided into a class of hard X-ray/radio-quiet Seyferts with emission spilling over into the soft γ-ray band, a class of MeV radio galaxies, and 3C 273, at redshift $z = 0.158$. This last object is an extraordinary ultra-luminous infrared galaxy and an AGN with a prominent blue bump, strong radio emissions and episodes of superluminal motion of radio emitting blobs observed with high-resolution VLBI[8] milli-arc-second radio imaging [24]. It was this source that heralded the γ-ray blazar class, whose existence was perhaps most clearly predicted by Königl [25] on the basis of its associated synchrotron and inverse Compton γ-ray emission.[9]

Fast-forwarding to 2015, the high-confidence clean sample of the Third Large Area Telescope Catalog of Active Galactic Nuclei (3LAC) [22] using the first four years of the Fermi-LAT data lists 1444 γ-ray AGN, divided into:

- $\approx 30\%$ FSRQs (404 sources);
- $\approx 40\%$ BL Lac objects (604 sources);
- $\approx 30\%$ blazars of unknown type (402 sources), which are *Fermi*-LAT high-latitude γ-ray excesses over the background associated with counterpart radio sources having inadequate optical follow-up to determine whether the source is a weak-lined BL Lac or strong-lined FSRQ;
- $<2\%$ non-blazar AGN (a mere 24 sources), which are mainly radio galaxies, radio-loud narrow line Seyfert galaxies, and candidate Seyfert AGN.

Besides black-hole powered AGN, the other main class of HE and VHE γ-ray galaxies are the star-forming galaxies whose high-energy activity is ultimately powered by the kinetic energy of exploding stars. In addition to the Milky Way, they include the Large Magellanic Cloud, detected with EGRET in 1992 [27], and the Small Magellanic Cloud reported by the Fermi-LAT Collaboration in 2010 [28]. The detection of star-forming galaxies outside the Milky Way and its satellites commenced with the joint announcement of Fermi-LAT [29] and VHE detections of NGC 253 [30] and M82 [31]. Fermi-LAT has since announced the detection of Andromeda, but no ultraluminous infrared galaxy (not counting 3C 273) has been detected at HE or VHE.

---

[8] VLBI: Very Long Baseline Interferometry.
[9] The importance of γ rays in extragalactic jet astronomy otherwise received little attention at that time [26].

The growth rates of the different primary source classes are plotted in Fig. 3 left. Combined efforts of the VERITAS, MAGIC, and H.E.S.S.[10] ground-based arrays has led to the explosion of new AGN sources at VHE (Fig. 3 right), importantly assisted by the all-sky capability of Fermi-LAT.

Excepting the local group galaxies and the starburst galaxies NGC 253 and M82, all other extragalactic VHE sources are AGN, most of them being radio-loud, but a few nearby radio-quiet Seyfert galaxies.[11] A complex background due to the Fermi bubbles [32] and possible background blazars has hampered the search for Fermi-LAT detection of the famous ultra-luminous infrared galaxy Arp 220.

BL Lac objects with peak synchrotron frequency of the νF_ν spectral energy distribution (SED) at UV and X-ray energies dominate the VHE sample of AGN. A smaller fraction of sources, including radio galaxies, have lower peak synchrotron frequencies. Almost all of the VHE AGN are also detected with the Fermi-LAT [22], allowing complementary studies of the SED over ≈ 6 orders of magnitude in energy, limited on the lower end, $\ll 100$ MeV, by poor sensitivity of MeV-regime telescopes, and on the higher end, $\gtrsim 10$ TeV, by γ-ray pair production attenuation with optical/IR photons of the extragalactic background light (EBL). Because BL Lac objects have weak lines, either due to an intrinsically weak accretion disk and BLR, or due to the BLR radiation being "washed out" by beamed nonthermal radiation [6], a large fraction of BL Lac objects, $\approx 50\%$, do not have precisely measured redshifts. Attenuation of γ rays with the EBL provides a technique to determine redshift [33], which can be used with a range of other techniques to constrain redshift [34,35]. The redshift incompleteness problem is a major issue in statistical studies of blazars.

2.1. Radio-loud blazars and model outlines

The prime AGN science for HE and VHE γ-ray astronomy is the science of radio-loud blazars. How radio-loud are these objects? A blazar's *apparent isotropic radio luminosity* $L_r = 4\pi d_L^2 \Phi_r$, where d_L is the luminosity distance[12] and Φ_r is the energy flux at radio frequencies, can reach $\approx 10^{39}$ W in powerful blazars such as 3C 454.3 and PKS 1510-089. Isotropic *bolometric* blazar luminosities dominated by HE γ rays can reach apparent values $>10^{43}$ W, as in the case of 3C 454.3 during a flaring state in 2010 November [36]. The blazar engine is required to generate large amounts of power irregularly over remarkably short timescales $\ll R_S/c$ (the Schwarzschild radius light crossing time), collimate the relativistic jet outflow, and amplify the received flux via Doppler boosting. Beaming corrections even as small as 0.1% make the energetics of anything other than an $\approx 10^9 M_\odot$ supermassive black hole infeasible. Note that the radio (i.e. $\lesssim 100$ GHz) luminosity L_r of the Milky Way is $\cong 2 \times 10^{31}$ W, ≈ 3 orders of magnitude less than the radio luminosity of the nearby FR-1 radio galaxy Cen A.

The two main classes of γ-ray blazars, namely FSRQs and BL Lacs, are usually defined according to conventional criteria according to which a blazar is a BL Lac object if the equivalent width of the strongest optical emission line is <5 Å, and the optical spectrum shows a Ca II H/K break ratio <0.4 in order to ensure that the radiation is predominantly nonthermal (the Ca II break arises from old stars in elliptical galaxies). The Fermi-LAT collaboration also introduced [37] a new blazar classification, alluded to earlier, based on the frequency $\nu_{\mathrm{peak}}^{\mathrm{s}}$ of the νF_ν synchrotron SED, with low-synchrotron-peaked (LSP) blazars having $\nu_{\mathrm{peak}}^{\mathrm{s}} < 10^{14}$ Hz, intermediate-synchrotron-peaked (ISP) blazars having 10^{14} Hz $< \nu_{\mathrm{peak}}^{\mathrm{s}} < 10^{15}$ Hz, and high-synchrotron-peaked (HSP) blazars for sources with $\nu_{\mathrm{peak}}^{\mathrm{s}} > 10^{15}$ Hz.[13] The FSRQ blazars are found to have mostly soft γ-ray spectra, with $\Gamma \geq 2.2$, and also to be in the LSP blazar class, indicating that their rapidly falling spectra are unlikely to provide significant fluxes at TeV energies. On the other hand, the type of BL Lac objects that are strong VHE sources, indicating that the peak energy of the γ-ray component is $\gtrsim 100$ GeV, are primarily HSP blazars.

Understanding the dynamic, broadband multiwavelength and multimessenger data from blazars depends on an underlying model. In the Marscher–Gear [38] model, sometimes referred to as a "shock-in-jet" model, a background plasma ejected along the jet axis, possibly moving outward at relativistic speeds, supports a shock that deposits nonthermal power in the form of electrons with a power-law spectrum. The flow magnetic field as a function of radius is parameterized, as is the electron injection power with radius. From this basis, the total radio emission or radio intensity as a function of time can be calculated for comparison with multi-band radio data [39] and interferometric images.

Surely a model like this must apply to outflowing plasma shocked by irregularities in the flow. Nevertheless, in contrast to the shock-in-jet model, a simpler "one-zone model" has been widely adopted as the standard paradigm for modeling the multiwavelength SEDs of blazars. In its simplest form, a spherical ball (in the fluid frame) of magnetoactive plasma entrains a nonthermal electron distribution. The magnetic field is assumed to be randomly oriented, and the pitch-angle distribution of particles is isotropic. Instabilities or shocks in these plasma blobs are thought to accelerate very energetic particles, which radiate photons whose flux is amplified in the jet axis along which the magnetoactive plasma travels at highly relativistic

---

[10] H.E.S.S.: High Energy Stereoscopic System, in Namibia; MAGIC: Major Atmospheric Imaging Cherenkov, in the Canary Islands; VERITAS: Very Energetic Radiation Imaging Telescope Array System, in Arizona.

[11] As of 2015 May, no GRB has been detected with a ground-based VHE instrument.

[12] The luminosity distance d_L is conventionally defined in such a way that the ratio of the absolute to the apparent luminosity (assuming isotropic emission) be equal to $4\pi d_L^2$.

[13] When redshift is unknown, the measured νF_ν peak synchrotron frequency is an uncertain factor $(1+z)$ smaller than the rest frame νL_ν peak synchrotron frequency.
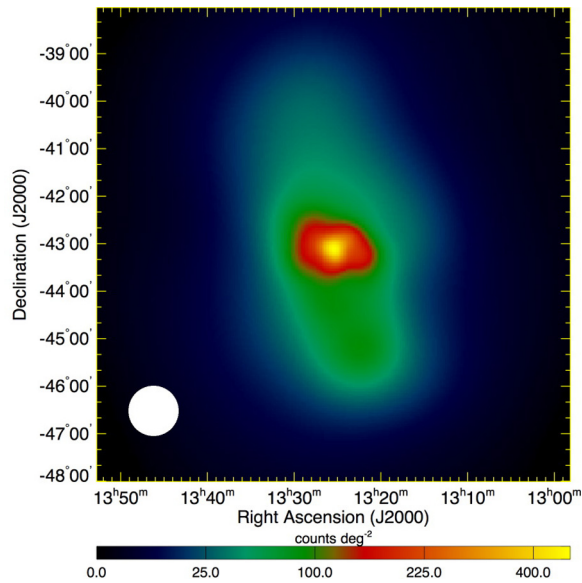
Fig. 4. The first γ-ray map of a radio galaxy. Fermi-LAT >200 MeV map of the radio galaxy Cen A, after subtracting point sources and the Milky Way's Galactic diffuse emission [40]. The angular extent of the γ-ray emission is $\approx 10°$. At a distance of ≈ 3.5 Mpc, these structures span ≈ 600 kpc.

speeds. The highly Doppler-boosted nonthermal electromagnetic emission is characterized by a double-humped SED in νF_ν representations, revealing much interesting blazar/black-hole astrophysics.

2.2. Radio galaxies

According to the unification scenario [4], as sketched in Fig. 2, radio galaxies are the misaligned counterparts of blazars. Conversely, blazars are radio galaxies in the circumstance when we happen to be looking down a black hole's jets. Therefore, radio galaxies and blazars are the same objects viewed from different directions. To complicate things further, the low-luminosity *Fanaroff and Riley* [5] FR1 radio galaxies showing twin-jet morphology are believed to be the misaligned counterparts of BL Lac objects, whereas the high radio-luminosity FR2 class of radio galaxies showing lobes and hot spots are thought to be the counterparts to the FSRQs, with a dividing line at a luminosity $L_{\text{rad}} \sim 10^{35}$ W. Establishing the underlying relationships between the aligned blazar and misaligned radio-galaxy classes is difficult because Doppler boosting of the jetted blazar emission means that blazars do not follow Euclidean behavior[14] either at low, moderate, or high redshifts. In the local universe, blazars are rare, with (an apparent) space density of BL Lac objects no greater than $\sim (10^2-10^3)$ Gpc^{-3}, whereas the density of the misaligned counterparts can be $\sim 10^3$ times greater, depending on the Doppler beaming factor.[15]

The first Fermi-LAT article [41] on misaligned AGN (MAGN) examined sources from the first LAT AGN Catalog (1LAC) [20] associated with steep (flux density $F_\nu \propto \nu^{-\alpha_r}$, with $\alpha_r > 0.5$) 178 MHz radio-spectrum objects in the Third Cambridge (3CRR) and Molonglo radio catalogs that show extended radio structures in radio maps. Because of the close relation between core dominance and γ-ray spectral properties, core dominance can be used to infer the alignment of radio-emitting AGN [42]. The original Fermi-LAT MAGN population comprises 11 sources, including 7 FR1 radio galaxies, namely, 3C 78 (NGC 1218), 3C 84 (NGC 1275), 3C 120, M87, Cen A, NGC 6251, and PKS 0625-354, two FR2 radio galaxies (3C 111 and PKS 0943-76), and two steep spectrum radio quasars (3C 207, 3C 380) that are thought to be slightly misaligned FSRQs.

The MAGN sources in the 3CRR catalog have large core dominance parameters compared to the general 3CRR source population, implying that the beamed component makes an appreciable contribution to the γ-ray flux. This is furthermore supported by the fact that four of these sources—3C 78, 3C 111, PKS 0943-76, and 3C 120—do not appear in 2LAC [21], evidently due to variability. By the time of the 3LAC, the population of MAGN has nearly doubled. One new source is IC 310, a head-tail radio galaxy or slightly off-axis FR1 radio galaxy [43] in the Perseus cluster with HSP BL Lac properties, that was detected by MAGIC [44] after being alerted of a Fermi high-energy excess [45]. Three others are Fornax A, an FR1 radio galaxy, and Pictor A and 3C 303, both FR2 radio galaxies. Fornax A and Pictor A were widely suspected of being sources of high-energy γ rays (e.g., [46]). Cen A is the first mapped radio galaxy at GeV energies, as shown in Fig. 4 [40]. The second

---

[14] If all sources with the same intrinsic isotropic luminosity were distributed uniformly in Euclidean space, the number N of sources with an apparent luminosity greater than S would vary like $S^{-3/2}$; for blazars, the slope of the cumulative distribution of $\log N$ versus $\log S$ does not have an index of -1.5.

[15] When the angle θ between the velocity βc of the radiative zone and the line of sight $\mathbf{n}$ is small enough, the frequency of the jet emission, which relativistic aberration confines within a half-angle of $\sim 1/\Gamma$ radians from β (with the Lorentz factor $\Gamma = (1-\beta^2)^{-1/2}$), is seen by the observer multiplied by a Doppler beaming factor $\delta = [\Gamma(1-\beta\cos\theta)]^{-1}$. This enhances significantly the observed flux by a factor $\sim \delta^4$ compared to what is expected from isotropic $1/r^2$ flux-dependency.
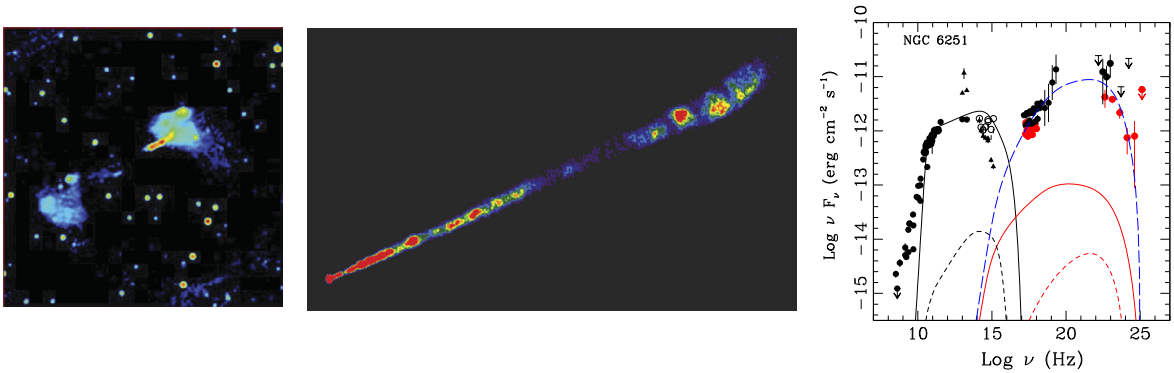
Fig. 5. Three views of the same object. *Left*: Radio image of NGC 6251 [51]. The image size spans 72.5′, which corresponds to a projected distance of ≈2.0 Mpc for an angular diameter distance of ≈98 Mpc. *Center*: High-resolution VLA image of the inner jet of NGC 6251, spanning a projected distance of ∼4 kpc [52]. *Right*: Multiwavelength spectrum of NGC 6251, with synchrotron self-Compton model fit [47].

extended radio galaxy at HE could be NGC 6251 [47], given its extended radio structure (at $z = 0.0247$ and a luminosity distance $d_L \cong 103$ Mpc, the angular extent of its radio emission is ≈0.8°; see Fig. 5).

Radio-loud Narrow Line Seyfert 1 (RL-NLS1) galaxies have also been established as a γ-ray source class [48]. These objects show narrow Hβ lines with FWHM line widths $\lesssim$2000 km·s^{-1}, weak forbidden lines ([$OIII$]/H$\beta < 3$) and a strong Fe II bump, and are therefore classified as narrow-line type I Seyferts [49]. By comparison with the $\sim$10$^9 M_\odot$ black holes in blazars, the host galaxies of RL-NLS1s are spirals that host nuclear black holes with relatively small ($\sim$10^6–10$^8 M_\odot$) mass that accrete at a high Eddington rate. The detection of these objects challenges scenarios where radio-loud AGN are hosted by elliptical galaxies that form as a consequence of galaxy mergers [50].

The misaligned AGN and radio galaxies now found to be HE and VHE emitters make it clear that there are particle acceleration and γ-ray emission sites far beyond the inner radio jet. The nearby giant radio galaxy M87 was the first non-blazar extragalactic VHE γ-ray emitter [53], followed later by Centaurus A and IC 310. While only Cen A was detected by EGRET, Fermi-LAT has found HE counterparts to all VHE radio galaxies and, in addition, discovered other HE-emitting radio galaxies [37,54]. The large radio structures in Cen A exceeds the field of view of IACTs, challenging conventional VHE detection that searches for point sources of radiation. The CTA observatory, however, with an order of magnitude improvement in sensitivity and better angular resolution, should greatly improve our knowledge of radio structures with extended VHE emission.

While Cen A does appear to have rather stable VHE emission, M87 and IC 310 have exhibited large and rapid flux variations. All current major IACT observatories are able to observe M87 quasi-simultaneously, and a joint effort was led in 2010 to search for variability on timescales shorter than a day, which is of the order of the light crossing time of the Schwarzschild radius for the supermassive central black hole in M87. Multiwavelength signatures appear to be different from previous occurrences of VHE flux enhancement, but an interesting pattern emerged, namely a very significant X-ray flux enhancement of the core during two such episodes [55]. Even faster flux variability was found in the radio galaxy IC 310, on time scales of a few min [56], shorter than the light crossing time across the event horizon. This has previously only been seen in HSP BL Lac objects.

2.3. Other galaxies

A keen interest is taken in both the HE and VHE regimes to uncover evidence of γ-ray emissions from classes of AGN other than those in the jet set (see Fig. 2). These "jet-deprived" AGN are not decorated with enormous radio displays. By lacking the jets, however, the less complex environment may allow a deeper view into the interior regions using optical and X-ray probes. Classes of X-ray missions, from the currently operating Chandra to the future Athena and ASTRO-H, provide deep insights into the inner accretion-disk geometry and behavior.

Out of the 24 "Other AGN" in the Fermi-LAT 3LAC clean sample [22], 13 are radio galaxies, discussed above, 5 are RL-NLS1 galaxies, 3 are steep spectrum radio quasars, and one (4C +39.23B) is a compact steep spectrum radio source (CSS), a category for which γ-ray emission has been predicted [57]. The low-latitude radio/γ-ray source PMN J1603-4904 may be another young, γ-ray emitting compact symmetric radio source [58]. The remaining two "AGN" out of the 24 are GB 1310+487 and PMN J1118-0413. Circinus, a Seyfert 2 galaxy, is located at $b = 3°$, so is not technically part of the LAT AGN Catalog samples because of the restriction to high ($|b| > 10°$) Galactic latitudes, though it would be another example of a radio-quiet galaxy possibly detected at γ-ray energies. Earlier Fermi-LAT searches for emissions from radio-quiet Seyferts [59], based on 120 bright hard X-ray radio-quiet Seyfert galaxies, obtained marginal detections of NGC 6814 and ESO 323-G077, neither of which is reported in the 2LAC and 3LAC. Incidentally, PKS 0943-76 from the MAGN catalog remains out of the 3LAC source list. The γ-ray emission from other candidate radio-quiet Seyfert galaxies or other AGN might be attributed to cosmic-ray interactions rather than radiations related to the central black-hole, but variability studies must contend with weak fluxes.
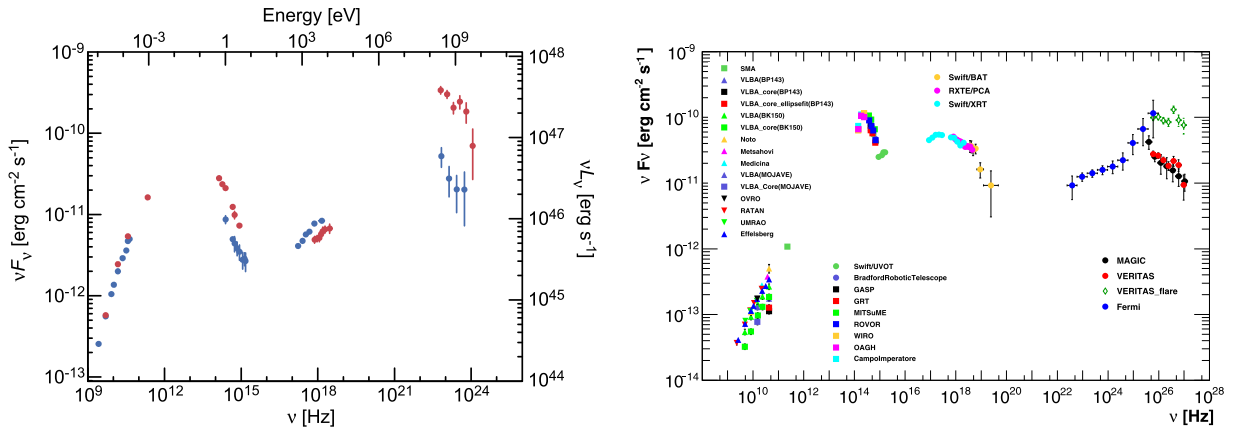
Fig. 6. Multiwavelength blazar SEDs. *Left*: Data shows two epochs of 3C 279 [62]. The red points were measured between MJD 54880 and MJD 54885, when a γ-ray flare was accompanied by a rapid change in optical polarization. *Right*: SED for Mrk 501 averaged over all observations taken during the multifrequency campaign performed between 2009 March 15 (MJD 54905) and 2009 August 1 (MJD 55044) [63]. The high-state flux detected by VERITAS from MJD 54952.9–54955.9 is shown by the green points, and this epoch is subtracted from the average SED. The legend reports the correspondence between the instruments and the measured fluxes. Galactic emission has not been removed.

3. AGN observed at high energies (>0.1 GeV) and very high energies (>100 GeV)

At high- and very-high energies, γ-ray emission is thought to be a by-product of black-hole nuclear activity that expels oppositely directed relativistic jets of plasma along the rotational axis of a spinning black hole. Most AGN activity is fueled by accretion, but the black hole's spin, which would be a consequence of the formation history of the galaxy and its central pc, could explain why only a small fraction, ~3%, of AGN have observable jets [60,23]. Morphological studies of the host galaxies of blazars are difficult because of the brightness of the nuclear light and the generally large redshifts, $z \gg 0.1$, of the host galaxies, particularly for FSRQs.

3.1. Multiwavelength SEDs of γ-ray blazars

Confining our attention to nonthermal jet radiation powered by black-hole activity, the most widely remarked feature of the broadband SEDs of γ-ray sources powered by black-hole activity is their two-humped shape. The characteristic double-humped SEDs of blazars extend over 15 or more decades in energy, from radio to TeV γ rays. Since blazars are intrinsically variable, observations are most valuable when they occur as nearly simultaneously as possible, in order to give an accurate picture of the AGN's emission across all wavelengths. Establishing an accurate SED is important to determine the relative importance of the different components in the continua, while the correlation of the variability in different wavebands gives insights into the jet physics. Multiwavelength observations are also sometimes the only available means to infer the nature of unidentified γ-ray sources, either through the characterization of the SED or, when a counterpart is found at different wavelengths, to correlate variability with the γ-ray flux variability. The high quality long baseline Fermi-LAT light curves for scores of blazars is a tribute to its large field of view and scanning strategy.

The most constrained instruments for multiwavelength (MWL) observations are usually the ground-based optical and VHE telescopes, which provide critical information on the radiative particles since the optical emission is often near the peak emission of the first hump in the SED, while the second probes directly the most energetic emission. The nonthermal optical emission is however often contaminated with optical emission from the host galaxy for objects with $z \lesssim 0.3$, while the γ-ray emission is attenuated through interactions with the cosmological optical and infrared backgrounds. The flux attenuation increases with distance and energy [61].

Fig. 6 shows the SEDs of two well known blazars, the FSRQ 3C 279 on the left and the HSP BL Lac object Mrk 501 on the right. It is also convenient to convert νF_ν into its equivalent in absolute luminosity: $\nu L_\nu = 4\pi d_{\mathrm{L}}^2 \times \nu F_\nu$, in which d_{L} is the luminosity distance. The distance modulus $D_{\mathrm{l}} = \log(4\pi d_{\mathrm{L}}^2)$ provides a simple conversion from νF_ν to νL_ν in a log–log representation.[16] The redshift of 3C 279 is $z = 0.538$, and during this epoch of observation the peak synchrotron frequency (in the source frame) is $\nu_{\mathrm{s}} \cong 10^{13}$ Hz. The value of νL_ν at $\nu = \nu_{\mathrm{s}}$ is $\nu_{\mathrm{s}} L_{\nu_{\mathrm{s}}} \cong 5 \times 10^{39}$ W $= 5 \times 10^{46}$ erg·s^{-1}, implying a bolometric isotropic synchrotron luminosity (supposing only a $1/d^2$ flux dependency) a factor ≈ 3 higher. The redshift of Mrk 501 is $z = 0.03366$, implying a distance of ≈ 149 Mpc and a distance modulus $D_{\mathrm{l}} = 54.42$. Its peak synchrotron frequency $\nu_{\mathrm{s}} \cong 10^{17}$ Hz and, from Fig. 6 and D_{l}, $\nu_{\mathrm{s}} L_{\nu_{\mathrm{s}}}^{\mathrm{pk}} \cong 10^{37}$ W (10^{44} erg·s^{-1}), so that the bolometric synchrotron flux is a factor $\approx 5\times$ larger (the width of the synchrotron SED in Mrk 501 is wider than that of 3C 279). Although the ratio of the

---

[16] Since c.g.s. units are used in most AGN SED's in the literature, d_{L} is here expressed in cm.
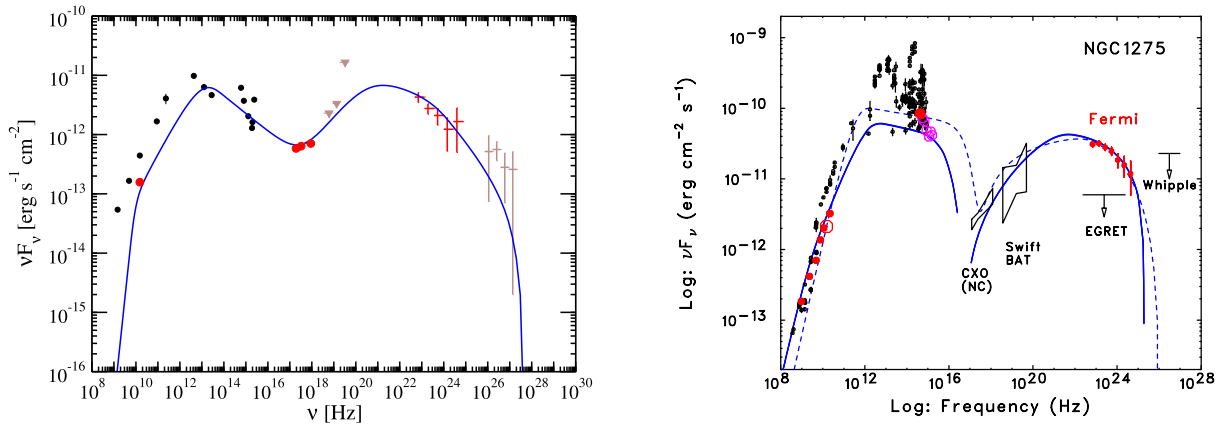
Fig. 7. Multiwavelength radio-galaxy SEDs. *Left*: SED data of M87 (where the TeV data from the HESS experiment are not contemporaneous with the Fermi-LAT data) and one-zone model fit [64]. *Right*: SED data for NGC 1275, including one-zone model fits [65].

synchrotron powers for the two blazars is $\sim$50, the ratio of the γ-ray powers can be $\gtrsim 10^2$ because of the large Compton dominance of the FSRQ's SED in γ rays.

Examination of the SEDs in Fig. 6 shows that several issues need clarification. Considering only AGN emission requires that any residual galactic continua be removed, as seen in the Mrk 501 SED that contains a strong IR feature from old stellar populations of the host galaxy. The examination of the correlated activity of the nucleus requires, in addition to simultaneity, either imaging or variability to identify these emissions themselves. Where imaging is not possible, timing steps in, with the presumption that the most luminous and highly variable radiations can only be produced by the nuclear black hole. For SED correlation studies measured over specified time windows, the most important observables are the measured frequencies ν_{pk}^s at the peak of the νF_ν synchrotron component, and ν_{pk}^C at the peak of the νF_ν inverse Compton component. In the source frame for a known redshift z, the peak frequencies are $\nu_s = (1 + z)\nu_{pk}^s$ and $\nu_C = (1 + z)\nu_{pk}^C$. The corresponding values νL_ν^s (respectively νL_ν^C) at peak synchrotron (respectively Compton) frequency are then deduced. The variability time t_{var} is crucial to spectral modeling, but is often the most elusive quantity to measure, because variable components may be hidden beneath a slowly varying continuum, and the variability at different energy ranges can be very different. Other important observables are the width and structure of the various components of the SED. As can be seen from the 3C 279 SED, the extrapolation of its X-ray emission to the γ-ray band is discontinuous, implying multiple emission components. In the simplest case, the same electrons would be responsible for the synchrotron emission and for the inverse Compton effect by upscattering their own synchrotron radiation (synchrotron-self Compton or SSC process). However, accurate modeling of detailed SEDs of FSRQs require both synchrotron self-Compton and one or more external Compton components.

Even in the absence of a blazar SED model, studies of the statistics of many blazars can be used to correlate the observables noted above. These correlations test blazar SED models and suggest relationships between different blazar classes. Significant blazar correlations have been established from statistical studies, as described in Section 6.

3.2. Multiwavelength SEDs of γ-ray radio galaxies

Most radio galaxies are of the FR1 class, including the radio galaxies detected at γ-ray energies, in which case their aligned counterparts are BL Lac objects, according to the unification scenario [4]. By comparison with FR2 and FSRQ galaxies, these are the simplest "one-zone" configurations, consisting of a ball of magnetized plasma entraining nonthermal electrons making synchrotron radiation together with SSC X-rays and γ rays. Indeed, early studies of radio quasars concluded that the lack of self-Compton X-rays was inconsistent with the assumption of a stationary emitting region or, more radically, either the nonthermal synchrotron interpretation for extragalactic radio sources was incorrect or redshifts were not cosmological. Emission regions moving at relativistic speeds preserved the cosmological interpretation of quasars. These plasma jets require black-hole engines, and furthermore provide the energy to form, over cosmic timescales, the extended radio lobes of radio galaxies.

Fig. 7 shows data for M87 [64] and NGC 1275 [65], along with spectral models of these radio galaxies. Fig. 5 also shows one-zone modeling for NGC 6251 [47]. An interesting result of SED modeling of radio galaxies is that their radio-through-γ-ray SEDs are generally well fit with large physical-dimension, slowly varying radio-emitting plasma moving at mildly relativistic speeds, with bulk Lorentz factor $\Gamma \sim 1.5$–2. Such small beaming requirements are at odds with the larger values of $\Gamma \sim 10$–30, more typical of those derived for the radiating relativistic jet plasma through BL Lac blazar spectral modeling, and suggest that emission regions with different velocities exist. Because of the powerful beaming $\propto \delta^6$ for

external Compton radiations,[17] the central rapidly moving jet emission is hardly seen at large angles from the jets. Instead, the γ-ray emissions from radio galaxies might be made in structured layers of the jet as in [38,66] and in the spine-sheath model [67], or could result from an extended emission region with varying Doppler factor as a result of jet deceleration [68]. See Ref. [47] for spine-sheath modeling of NGC 6251.

4. Variability properties of γ-ray blazars

The dimension of time introduces all sorts of complexities into blazar physics. Indeed, it was the rapidly variable radio fluxes, on time-scales of months, that introduced the blazar puzzle [69,70]. Blazars, as the name implies, are highly variable sources, yet their variability properties are frequency- and class-dependent, and highly resistant to the identification of any simple underlying patterns or behaviors. First is the question of what constitutes variability. The likelihood of fluctuations away from an average value is something that can be determined quantitatively from a given data set. Auto-correlation analyses can identify preferred time scales. Cross-correlation analyses can constrain jet models and identify consistent particle acceleration and radiation processes. Predictions about correlated emissions or changes in fluxes at different frequencies test jet models.

4.1. γ-Ray variability

Day-scale γ-ray variability of blazars was known from the EGRET era, most notably from the 1991 August flares of 3C 279 [71]. Fermi-LAT, with its better sensitivity, can probe variability on much shorter time scales. But for only a few blazars does Fermi-LAT have sensitivity to probe to a few hour time scale during major outbursts, namely 3C 454.3 [72], PKS 1222+216 [73], PKS 1510-089 [74,75], and 3C 273 [76,77]. These few hours are in the ball park of simple expectations for minimum variability time scales for supermassive black holes. Only recently has evidence for variability at sub-ks timescales at GeV energies been found in flares of 3C 279 and PKS 1510-089 [78].

Most simply, the natural scale of the blazar engine is the Schwarzschild radius R_S of a black hole with mass M_{bh}, corresponding to a light-crossing time of:

$$R_S/c \cong 10^4 \text{ s} \times M_9 \text{ where } M_9 = M_{bh}/10^9 M_\odot . \tag{1}$$

Supermassive black holes with masses $\approx 10^9 M_\odot$ are supposed to power most blazars; black-hole masses in blazars are obtained, e.g., by the bulge/black-hole mass relationship [79]. BL Lac objects, for instance, are almost entirely hosted in otherwise normal elliptical galaxies [80], so that the bulge mass is essentially equal to the host galaxy's normal matter mass, implying $\sim 10^9 M_\odot$ black holes at their centers. It seems reasonable to expect a loss of power at smaller timescales than $\cong$3 h, as flaring on time scales shorter than R_S/c should reduce the size of the implied emission volume and with it, the radiant luminosity. Yet powerful flares varying on timescales $\sim 100\times$ shorter than implied by Eq. (1) have been detected in VHE; mainly from HSP BL Lacs.

Hints of ultra-rapid variability in blazars were evident in early Whipple data of Mrk 421 [81], and in data from successor VHE telescopes preceding the era of γ-ray Cherenkov arrays. But it was with the operations of the H.E.S.S., VERITAS and MAGIC VHE γ-ray observatories that measurements of extremely rapid variability of BL Lac objects began to threaten simple kinematic understanding of black-hole physics, presenting a puzzle that still remains today. Variability on time scales as short as $\approx$5 min in PKS 2155-304 [82], and a few min in Mrk 501 [83] and Mrk 421 [84], has now been reported by VHE telescopes.

Fig. 8, left and lower right, shows the extreme flaring behavior of PKS 2155-304 [82], measured with H.E.S.S. on and around 2006 July 28. At its most intense phase, factor-of-two flux variations are seen on times as short as 5 min. With apparent luminosities of the γ-ray component exceeding $\sim 10^{39}$ W and γ rays with energies as large as $\sim$3 TeV, $\gamma\gamma$ opacity arguments require bulk Lorentz factors $\Gamma \gtrsim 50$ [87]. Though most HSP BL Lacs display erratic and flaring outbursts, a class of HSP blazars has been established that show weakly or non-detectable VHE fluxes. Fig. 8, upper right, shows the H.E.S.S. light curve of 1ES 0347-121 [86], which, in this figure, shows no significant evidence of variability. VERITAS results on the HSP blazar 1ES 0229+200 ($z = 0.1396$) also shows extremely weak variability [88].

Rapid variability does not appear to be peculiar to the TeV BL Lac objects. The FSRQ 4C +21.35 has varied at 70–400 GeV energies on timescales as short as 30 min [89]. By comparison, significant MAGIC VHE detections of 3C 279 took place on two successive days, 22 and 23 February 2006 [90], after which it was also detected during a flare on 16 Jan 2007 [91]. The VHE fluxes for the two days in 2006 were each significant, and differed by $>2\sigma$, indicating day-scale variability for VHE emission from 3C 279.

Just preceding the launch of the Fermi Large Area Telescope, the satellite experiment AGILE,[18] with HE sensitivity comparable to EGRET, found that the FSRQ 3C 454.3 ($z = 0.859$) was "ringing off the hook" [92]. When Fermi LAT started monitoring the sky, with science operations starting in August of 2008, 3C 454.3 provided a wealth of information from γ rays alone on its variability properties. For example,

---

[17] δ is the Doppler beaming factor mentioned above.
[18] Astro-Rivelatore Gamma a Immagini L'Eggero, an Italian Space Agency project launched in April 2007.
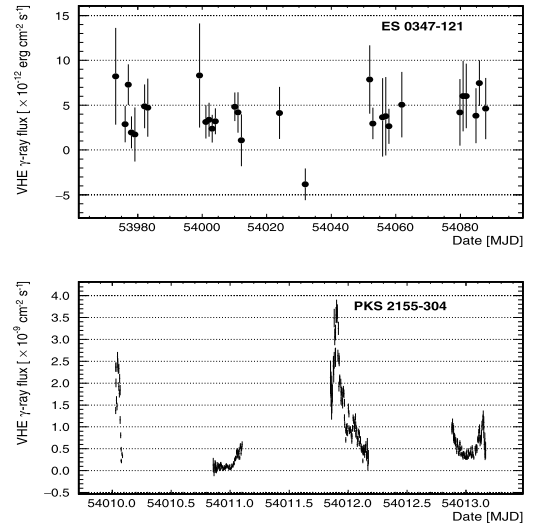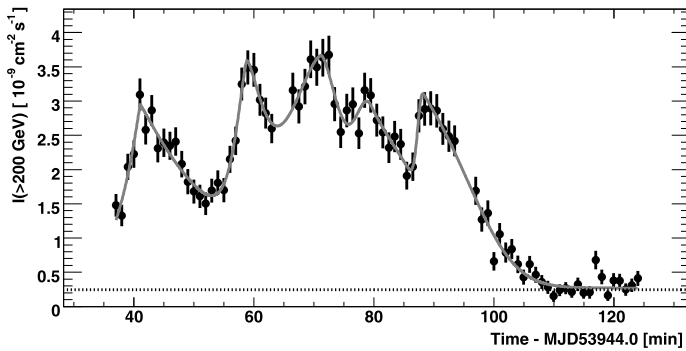
Fig. 8. BL Lac light curves. Light curves of the HSP BL Lac object PKS 2155-304 ($z = 0.116$) in 2006 July 28 (left) [82] and during the period of the 2006 flares (lower right) [85]. H.E.S.S. VHE light curve of the HSP BL Lac object 1ES 0347-121 ($z = 0.815$; upper right) over a period of ~ 120 days [86].

(i) a broken power-law function to model the Fermi-LAT spectrum of 3C 454.3 shows a spectral break at $E_{\rm br} \cong 1.5$–3 GeV (observer's frame) [93], similar in energy in the source frames for the spectral breaks of other LSP and ISP blazars [94];

(ii) $E_{\rm br}$ is only weakly dependent (showing slight evidence for a hardening) on increasing GeV flux [95];

(iii) there seems to be a plateau phase preceding flares and a tendency for highest energy photons to come later in the flare [95];

(iv) the largest flare reached apparent isotropic γ-ray luminosities $L_\gamma \approx 2 \times 10^{43}$ W [72], eclipsing the EGRET record for PKS 1622-297 [96].

A Fermi-LAT study of blazar variability [97] shows that FSRQs are more variable than BL Lac objects in the GeV range, even taking into account flux differences. The power density spectrum of light curves of bright blazars are generally well fit with power-law power density spectra.

4.2. Multiwavelength variability

Multiwavelength campaigns provide valuable information to answer questions concerning the location and environment of the blazar γ-ray emission site, which are frustratingly uncertain. The precise location can, of course, depend on the particular blazar and whether it is in a flaring or quiescent state. Nevertheless, depending on the blazar model, some answers to the question about the location of the usual γ-ray emission site in FSRQs are:

– the deep inner jet, where abundant highly ionizing radiation is found [98,99];
– the sub-pc scale of the BLR [100,101];
– the pc-scale where the IR radiation from the dusty torus dominates [102];
– the $\gtrsim 10$ pc scale where external radiation fields weaken;

Radio/γ-ray correlations can be used to infer how far the γ-ray emission site is from the central black hole, and such studies often infer that the γ rays are produced at many pc removed from the black-hole engine [103].

Two of many possible examples of multiwavelength blazar studies are shown in Fig. 9. On the left, light curves at radio, X-ray, optical, and γ-ray frequencies for the FSRQ PKS 1510-089 are shown [104]. Besides being one of only 3 VHE FSRQs now known, and showing GeV variability on timescales < 3 h [74,78], optical polarization and electric vector polarization angle can be monitored. In PKS 1510-089, a large swing of the electric vector polarization angle accompanies the optical and γ-ray flaring, with the polarization fraction reaching 30% [104]. Clearly there is an ordered magnetic field disrupted by the flaring activity. Marscher et al. [104] argue that this points to events taking place past the optically thick radio core, implying a distant, $\gtrsim 10$ pc location of the γ-ray emission site in sources like PKS 1510-089, and the LSP BL Lac objects OJ 287 ($z = 0.305$) [105] and AO 0235+164 ($z = 0.94$) [106] (neither of which has been detected at VHE). Impressive optical polarization angle swings correlated with γ-ray flaring activity in 3C 279 have been reported by the Fermi-LAT collaboration [62], leading to much speculation about the jet's magnetic-field geometry ranging from turbulent ejection to helical motions of the emitting plasma to bent jets.

The radio/γ-ray connection is of particular interest because there is wide agreement that these radiations are fully nonthermal, as compared with IR, optical, and X-ray, which can include quasi-thermal dust and accretion-disk emissions.
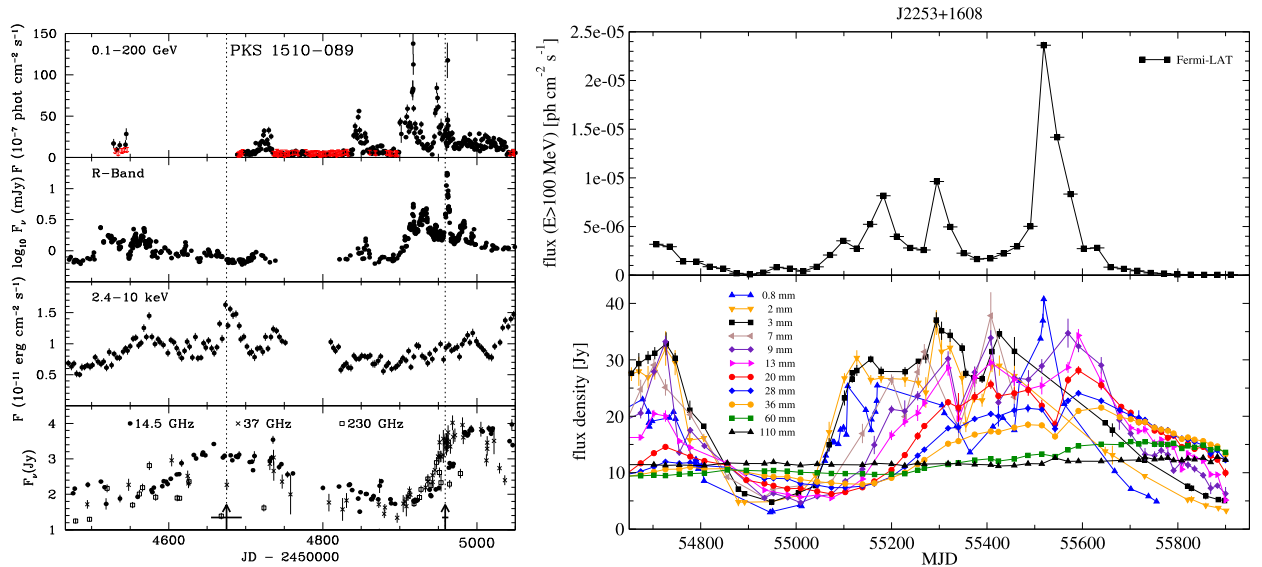
Fig. 9. Multiwavelength FSRQ light curves. Multiwavelength flaring behavior of PKS 1510-089 (*left*; $z = 0.36$) [104] and 3C 454.3 (*right*; $z = 0.86$) [39].

Fig. 9, right, shows radio and γ-ray light curves for 3C 454.3, also known as 2253+1608 [39]. Cross-correlation of the cm to sub-mm light curves with the γ-ray light curves of 3C 454.3 and several other blazars reveals a frequency-dependent lag of the radio with respect to the γ rays, with longer lags at longer wavelengths. The cm wavelength emission lags the radio by ≈ 2 months, in agreement with earlier claims [107]. Detailed studies of the radio-γ-ray connections in blazars are conducted at the Owens Valley Radio Observatory [108].

4.3. Extreme flaring states

The long-term average SEDs of FSRQs and low-peaked BL Lac objects generally display a spectral softening above a few GeV [94]. Some of the models to explain this softening involve combined accretion-disk/BLR scattering by jet electrons [109], Klein–Nishina effects at a few GeV when jet electrons scatter Ly α radiation [100], or $\gamma\gamma$ attenuation of γ rays made deep in the BLR by He II Ly α and recombination radiation [98,99]. Episodes of extreme blazar flaring, where hard emission extends to $\gtrsim 10$ GeV without a break, challenge FSRQ SED models. Such extreme flaring states have been observed in the FSRQs PKS 0805-08 ($z = 1.84$), 3C 454.3 ($z = 0.86$) [110], and 3C 279 ($z = 0.538$) [111]. The rapid 30-min flaring time scale of VHE emission observed from PKS 1222+216 (4C +21.35) by MAGIC and Fermi-LAT [89,73] also challenge scattering models [112]. To reach VHE energies requires scattering of IR photons, as the scattering of BLR radiation faces both the decline of the cross section and the limit to scattered energy for Compton scattering in the Klein–Nishina regime.

Monitoring the full sky for GeV γ-ray transients requires a large field-of-view instrument, like Fermi-LAT, in its standard scanning mode. HAWC provides a weaker version of the same capability at TeV energies. Fermi all-sky variability analysis of 47 months of Fermi-LAT data reveal ~ 27 sources at low galactic latitude that are likely to be blazars [113]. Triggers for ground-based telescopes sensitive to the VHE part of the spectrum, and real-time alerts for blazar γ-ray hot spots still rely, unfortunately, on luck and the phase of the moon, though technologies replacing photomultipliers with photodiodes are being developed to mitigate the latter problem [114], at least for the brightest sources.

5. Statistical properties of γ-ray blazars

Fundamental progress can be made by identifying a significant empirical correlation that can then be understood theoretically. This is the basis of the Hertzsprung–Russell diagram in stellar astronomy relating stellar luminosity and temperature. An analogous relationship in blazar physics would relate synchrotron or Compton luminosity $L_{s(C)}$ to "temperature," of which the synchrotron ($\nu_s = \nu^s_{peak}$) and Compton (ν_C) peak frequencies are analogs in the nonthermal universe. This is the basis of the blazar sequence, described next, followed by other robust correlations in blazar γ-ray astronomy.

5.1. Blazar sequence

The luminosity of the lower-energy synchrotron hump in the SED of blazars appears to anti-correlate with the peak synchrotron frequency ν_s, as shown in the left panel in Fig. 10 [115]. The sample used in Ref. [115] to construct this diagram is generally composed of powerful, LSP FSRQs and weaker, HSP BL Lac objects. A recent analysis of the blazar sequence [116] notes that a set of blazars simulated by standard one-zone models (i.e. a single Lorentz factor and a convex electron
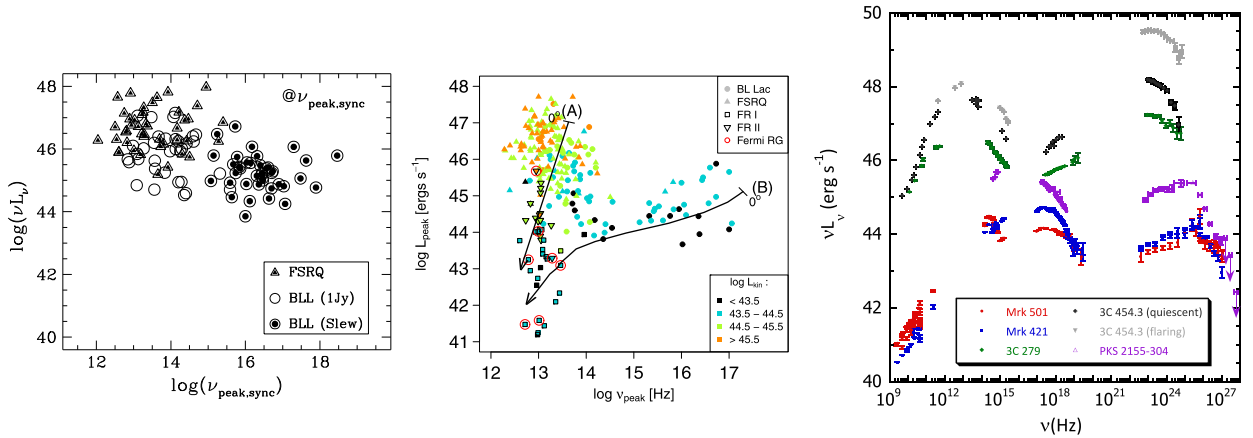
Fig. 10. Three versions of the blazar sequence. Left figure is the original blazar sequence diagram presented by Fossati et al. (1998) [115]. Center figure is the more recent version presented by Meyer et al. (2011) [116], including radio galaxies. Right figure shows quasi-simultaneous multiwavelength blazar νL_ν SED for Mrk 421, Mrk 501, PKS 2155-304 [117], 3C 279 (Epoch C from [118]) and two epochs of 3C 454.3 [100]. The blazar sequence showing the anti-correlation of bolometric synchrotron and Compton luminosities with peak synchrotron and Compton frequencies, respectively, can be deduced from the plot.

spectrum) at a range of observation angles yields a corresponding diagram in strong contradiction with the sequence of the left diagram of Fig. 10. Such one-zone blazar models would predict $L_{\mathrm{syn}} \propto \nu_s^4$ (and $L_{\mathrm{syn}} \propto \nu_s^3$ for a standing shock [119]). Nevertheless, a low-luminosity, low-frequency extension must be found in the L_{syn} vs. ν_s plane from the off-axis emissions of blazars. Yet the overall behavior of the blazar sequence is orthogonal to this.

As updated by [116], the blazar sequence forms an "L" or even a "y," as shown in the center panel of Fig. 10. This suggests two separate populations, which are further distinguished by the jet kinetic powers inferred from the luminosities of the extended radio emissions around radio galaxies and the host galaxies of blazars. The highest luminosity objects are invariably LSP FSRQs, and the lower-luminosity objects are mostly HSP BL Lac objects. The trends which appear for these objects are compatible with what is expected from rapid angular debeaming in a strong and homogeneous jet for FSRQs (track A in Fig. 10) and less rapid debeaming in the case of BL Lacs having weaker jets and velocity gradients (track B in Fig. 10). The radio galaxies occupy the positions expected from the off-angle tracks of FSRQs and low-synchrotron peaked BL Lac objects.

This trend can be inferred from the associated blazar SED sequence illustrated in the right panel of Fig. 10. Note that a mixture of quiescent and flaring states are shown there, and that the blazar sequence is generally plotted from blazar SEDs averaged over long times, though it would be interesting to compare with flaring states. The transition from LSP to HSP objects was interpreted [120] as a result of decreasing Compton cooling associated with the decreasing energy density of the external radiation fields. This in turn allows an increase of the maximum electron energy, shifting the synchrotron and Compton peak emissions blueward. Smaller external radiation energy densities are attributed [50] to smaller accretion powers, which occurs when the circumnuclear environment of supermassive black holes is gradually depleted and hence less accretion-disk radiation is reprocessed. This trend is also reproduced by [121], who used as parameters the magnetic field of the blazar jet emitting region, the external radiation field energy density, and the jet angle to the line of sight.

The HSP population from low to high values of ν_s displays a contrary trend where L_{syn} is positively correlated with ν_s. This is argued [116] to be a consequence of a decelerating flow that explains the apparent contradiction between the large Doppler and Γ factors inferred from spectral modeling and $\gamma\gamma$ opacity arguments applied to BL Lac objects compared to the smaller values found from spectral modeling of radio galaxies and from VLBI observations of BL Lac objects at the milli-arc-second scale [116]. Intermittent black-hole ejecta with a variety of Γ values, followed by colliding shells, could make a decelerating jet in a colliding shell-type scenario. Radiative processes would, however, seem to provide a feedback mechanism in objects whose photon power is dominated by external Compton processes. The external Compton processes provide radiative braking, unlike synchrotron and SSC emissions in BL Lac objects, where the radiation is emitted isotropically in the jet frame.

5.2. Blazar divide

Another blazar correlation discovered in the Fermi-LAT data is a divide separating BL Lac and FSRQ-type blazars, when the γ-ray number spectral index Γ_γ, or the energy spectral index α_γ, measured in the 0.1–100 GeV energy range, are plotted as a function of γ-ray luminosity L_γ [122,20]. The version shown in Fig. 11 is from the 2LAC [21]. In the analysis of the Fermi-LAT data, the γ-ray spectral index Γ_γ is determined from a single power-law fit to all the data in the 0.1–100 GeV range, though the energy flux is determined by separate power-law fits in five energy bands (0.1–0.3, 0.3–1, 1–3, 3–10, and 10–100 GeV).
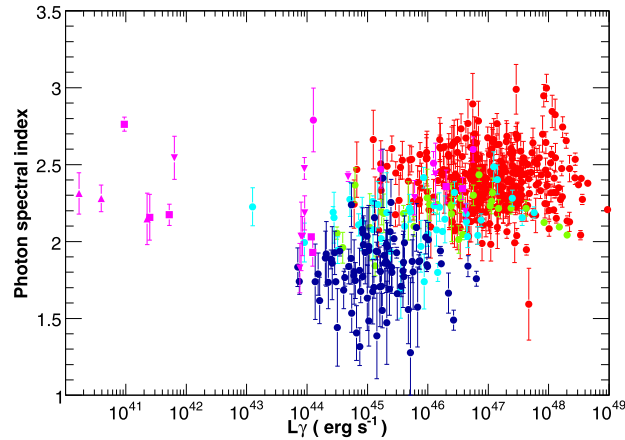
Fig. 11. The blazar divide. The photon index Γ_γ is plotted against γ-ray luminosity at γ-ray energies 0.1–100 GeV [21]. Red: FSRQs, green: LSP–BL Lac objects, light blue: ISP–BL Lac objects, dark blue: HSP–BL Lac objects, magenta: non-blazar AGN (circles: NLS1s, squares: misaligned AGN, up triangles: starbursts, down triangles: other AGN). The blazar divide refers to the abrupt change in spectral index between FSRQs and HSP BL Lacs at $L_\gamma \approx 10^{46}$ erg·s^{-1} (10^{39} W).

As can be seen, most FSRQ have $\Gamma_\gamma > 2.2$ and $L_\gamma > 10^{39}$ W (10^{46} erg·s^{-1}), while the BL Lac class is mainly in a region where $\Gamma_\gamma < 2.2$ and $L_\gamma \lesssim 10^{39}$ W (10^{46} erg·s^{-1}). A rather neat separation between these two classes takes place at $L_\gamma \sim 10^{39}$ W (10^{46} erg·s^{-1}), and is therefore known as the *blazar divide*. This divide is interpreted [122] as having a physical origin, possibly reflecting a transition to an accretion regime where the radiatively inefficient and low Eddington accretors have low γ-ray luminosities [123]. This is consistent with an interpretation where the inner edge of an optically thick, geometrically thin accretion disk moves out in radius with declining mass-accretion rate. Within the regions between the inner edge of the thin disk and the black hole is an advective flow, possibly with a hot X-ray emitting corona. The transition between the weaker, advection-dominated, low-radiative efficiency accretion flows, to the high-luminosity, high-radiative efficiency inflows at an Eddington ratio of $\sim$1% could explain the divide.

Except for a transition of the spectral index over a rather restricted range of apparent γ-ray luminosity L_γ, Γ_γ is insensitive to the value of L_γ. It is apparent from the distribution of FSRQs and BL Lac objects with peak synchrotron frequencies ν_s that a correlation between Γ_γ and ν_s follows. Modeling a large sample of blazars yields parameters that can then be correlated, such as the comoving electron Lorentz factor at the peak of the SED, making synchrotron photons with frequency ν_s. Ref. [124] argue that this distribution is consistent with a cooling scenario.
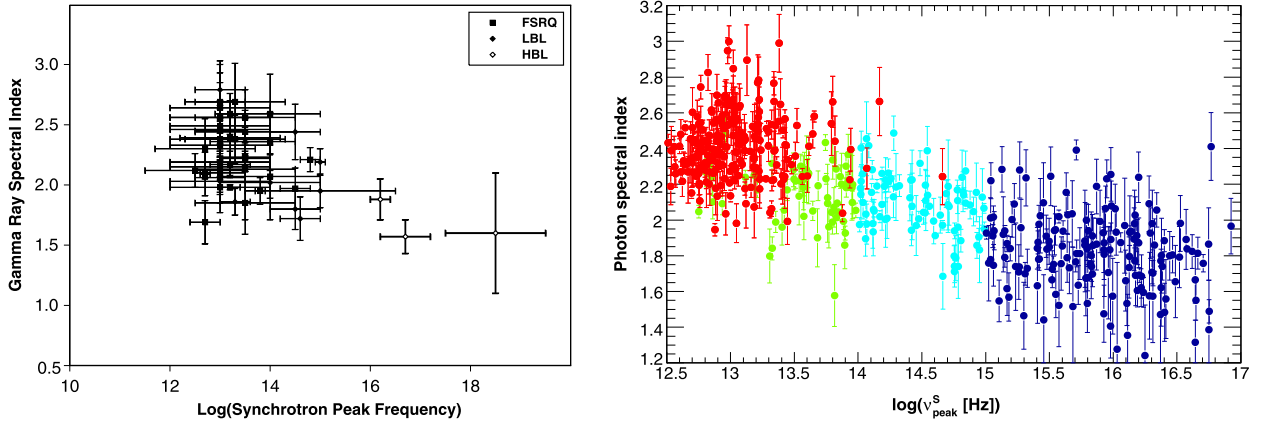
5.3. Spectral-index diagrams

A further robust correlation in blazar physics are the blazar spectral-index diagrams relating Γ_γ with either the peak synchrotron frequency ν_s or peak Compton frequency ν_C. The size of the Fermi-LAT sample and the improvement of the energy resolution over previous instruments now shows a clear correlation between the photon spectral index Γ_γ of HE AGN and ν_{peak}^s (Fig. 12). On the left is an early attempt to construct such a diagram from the EGRET data [125], and on the right is Fermi-LAT data from the 2LAC showing the strong correlation of Γ_γ with ν_s. The general trend can be described by the simple relation

$$\Gamma_\gamma \cong d - k \log \nu_s, \tag{2}$$

where d and k are constants. The corresponding highly correlated Γ_γ vs. ν_C can also be found in Fig. 29 of [126]. The ratio of the γ-ray and synchrotron peak luminosities gives the Compton dominance A_C, which can be plotted as a function of ν_s or ν_C. The A_C vs. ν_s plot is known to be highly correlated [115], and recent data shows that it displays an "L" shape [121] consistent with the blazar sequence diagram of Ref. [116] shown in Fig. 10.

This correlation can be explained [127] assuming an equipartition model[19] with a log-parabola electron energy distribution (i.e. an electron energy density $N(E) \propto E^{a+b \log E}$, [101]), noting that the synchrotron, SSC, and external Compton radiations in the Thomson regime produce a broadened log-parabola SED, the slope of which in the γ-ray domain is a function of the form of eq. (2) [128]. Note that the peak synchrotron frequencies of FSRQs appear clustered in the range $10^{12.5}$ Hz $\lesssim \nu_s \lesssim 10^{13.5}$ Hz. Another interesting feature of Fig. 12, right, is that the photon spectral indices do not reach values significantly smaller than $\Gamma_\gamma = 1.5$, which is near the flattest spectral index predicted in shock acceleration models [129].

---

[19] The model assumes equipartition between non-thermal electron and magnetic-field energy densities.

Fig. 12. Spectral index versus peak synchrotron frequency. *Left:* Spectral-index diagram based on the EGRET sample with 50 AGN [125]. *Right:* Spectral-index diagram based on the Fermi-LAT sample of 886 AGN from [37] (Red: FSRQs, green: LSP–BL Lacs, light blue: ISP–BL Lacs, dark blue: HSP–BL Lacs). The Fermi-LAT results clearly show that the HE γ-ray spectral index Γ_γ becomes harder when ν_{peak}^s increases, giving the significant correlation apparent in this figure.
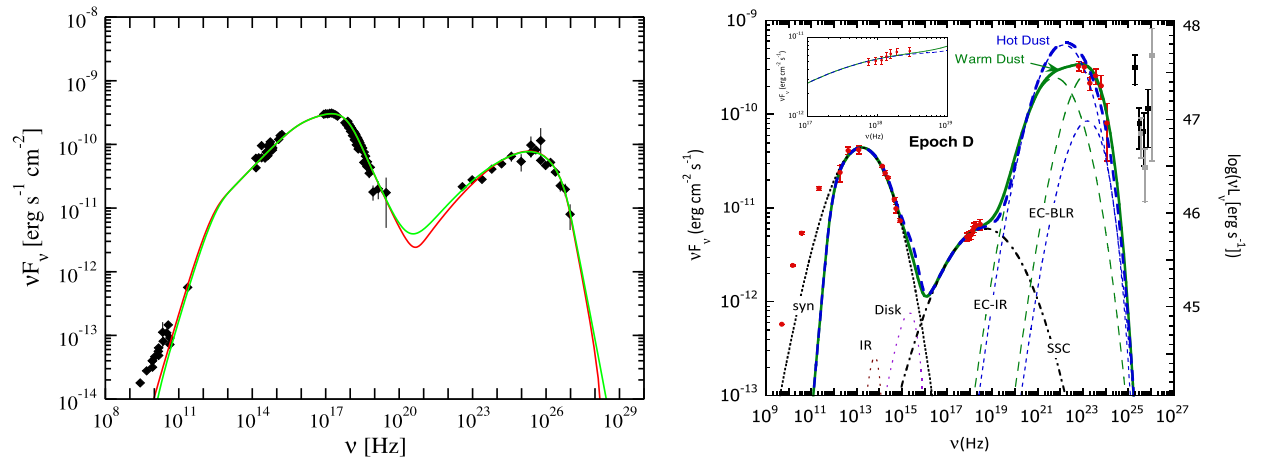
Fig. 13. Blazar model SEDs. *Left:* SED of Mrk 421 measured in multiwavelength campaigns including Fermi and MAGIC γ-ray telescopes [132]. Two one-zone model fits are shown, with $t_{\text{var}} = 1$ h and 1 day for the green and red curves, respectively. *Right:* Data show Epoch D SED of 3C 279 [118]. Blazar model fits [101] show separate spectral components in the fit, including the IR torus and accretion-disk emission, beamed synchrotron (syn), SSC, Compton-scattered IR (EC-IR) radiaion for warm and hot dust, and Compton-scattered BLR radiation (EC-BLR). Non-simultaneous VHE MAGIC data for 3C 279 [91] are shown for comparison. Total emission spectra include synchrotron self-absorption. Inset shows detail of fits at X-ray energies.

6. Blazar models

The blazar paradigm and astrophysics of blazar spectral modeling have been recently reviewed [130,23,131]. What may be worth noting in addition to the information found there is that the way in which the electron energy distribution (EED) is established is one of the distinctive features of a blazar model, and so should be well understood. As to theoretical efforts to understand γ-ray and multiwavelength results, perhaps most useful models are spectral and, in the best case, dynamical. There has been tremendous theoretical and modeling progress throughout the CGRO and Fermi-LAT eras, in parallel with advances in ground-based VHE astronomy, to measure quasi-simultaneous blazar spectra across a broad wavelength range. These data test the models, and a model that cannot be tested is not very useful.

Fig. 13, left, shows synchrotron/synchrotron self-Compton (SSC) spectral modeling [132] applied to Mrk 421, the prototypical HSP BL Lac. Adequate fits can be obtained from conventional one-zone SSC models with an EED described by a broken power law with exponential cutoff, or with a log-parabola EED. In comparison, Fig. 13, right, shows data for an epoch D (corresponding to the brightest γ-ray flare) SED of 3C 279 [118]. An approach [101] assuming a log-parabola EED and near-equipartition conditions between nonthermal electron and magnetic-field energy density gives the spectral models for epoch D as shown.

6.1. Leptonic models

The models shown in Fig. 13 are leptonic, and leptonic models are in most cases able to give good fits to multiwavelength blazar SED data. But even in the case of 3C 379, as shown by the non-contemporaneous MAGIC data [91] shown there, the observation of a VHE flare can strain a leptonic model, or at least lead to predictions regarding the properties of the synchrotron component, because the hardened electron distribution from a VHE flare should show up in the synchrotron SED.

A wide range of leptonic blazar spectral models have emerged in the last 20 years covering the most important aspects of jet physics. Any leptonic blazar model must comprise, in rough order of decreasing importance, the following features:

– relativistic boosting;
– electron energy distribution;
– magnetic field;
– synchrotron radiations;
– synchrotron self-Compton radiations;
– external Compton radiations;
– synchrotron self-absorption;
– accretion-disk and IR torus emissions;
– internal $\gamma\gamma$ absorption;
– direct accretion-disk photons (important when the γ-ray emission region is within 100–1000 R_S;
– external extragalactic background light (EBL) absorption [61];
– EBL-induced cascade radiations (or assumptions about the minimum intergalactic magnetic field) [61];
– external source $\gamma\gamma$ absorption (e.g., in the inner jet environment);
– cascade radiation spectrum from pairs formed by internal absorption;
– higher-order radiative processes, e.g., bremsstrahlung, ionization losses, etc.;

leaving aside the details of the particle acceleration mechanism, whether dynamic or snapshot modeling is being simulated, and the statistical method to fit data. And this leaves out a whole plethora of additional interesting complexities when hadrons are in the mix, as described next. The issues associated with leptonic blazar modeling of γ-ray sources have kept astrophysicists busy since 1992.

The short timescale puzzle mentioned above, in Section 5, has motivated work into magnetic reconnection and jets-within-jets models. In magnetic reconnection models [133], the short variability time is realized by an electron beam driven by reconnection taking place in a sub-volume of a larger region whose size scale is related to the Schwarzschild radius, R_S. To compensate for the small comoving size $R' = f\Gamma R_S$, with $f < 1$ implied by observations, reconnection is assumed to drive relativistic outflows or beams of particles with sufficiently large Lorentz factor that Doppler boosting compensates for the smaller available energy content in the small blob. The observed luminosity $L_{obs} \cong L_{iso} f^2 \left(\delta_p/\delta_j\right)^4$ so, provided that the plasma Doppler factor δ_p and jet Doppler factor δ_j are suitably chosen, the large apparent power is preserved even from the smaller size scale of the region. Other approaches include jet-within-jet or turbulent cell models [134–136], and Poynting-dominated jet models [137]. Plasma instability-induced short variability behavior has also been considered [138].

6.2. Hadronic models

An additional hadronic component could "rescue" a one-zone model by providing a γ-ray component from cosmic-ray proton- or ion-induced radiations in the blazar jet. So-called "orphan flares," as in the Whipple flare observed from 1ES 1959+650 [139], that show up in the γ-ray component, but lack corresponding counterpart flares expected from leptonic processes, have been used to implicate hadronic processes [140]. To the opposite of leptonic processes, hadronic components would leave no corresponding feature in the synchrotron part of the SED, because the γ rays made by proton and ion synchrotron processes would be in the GeV–TeV range, and the photon-lepton cascades induced by photopion production p, A + γ → p, A + π would cascade down to γ rays, with no direct effect on the synchrotron component. Ultra-relativistic protons accelerated by the blazar that reach intergalactic space can induce photopion secondaries within a few hundred Mpc by interactions with cosmic microwave background photons, and photopair secondaries over one or two Gpc through interactions with photons of the EBL [61,141,142]. These emissions can produce an anomalous γ-ray cascade component that could confuse attempts to measure the extragalactic optical and infrared background using $\gamma\gamma$ attenuation with the EBL. Such weakly variable VHE components may produce the SED of weakly variable BL Lac objects, like 1ES 0347-121 shown in Fig. 8.

Proton/ion synchrotron radiation provides one hadronic mechanism that could be important in blazars, but essentially requires a highly magnetized jet. The more favored hadronic mechanisms in blazars are photohadronic processes. One line of evidence that these processes operate in blazars depend on the detection of high-energy neutrinos, and whether they could account for some of the PeV or lower energy (30–500 TeV) IceCube neutrinos [143]. Tentative evidence linking radio/γ-ray blazars to IceCube neutrinos is given in Ref. [144].

6.2.1. Proton/ion synchrotron radiation

We derive (or rederive) magnetic-field and particle-energy requirements for proton- and ion-synchrotron radiation. The particle energy-loss rate by synchrotron radiation, averaged over pitch angle, is (primed parameters are in the frame comoving with the plasma)

$$-(\frac{\mathrm{d}E'}{\mathrm{d}t'})_{\mathrm{syn}} = \frac{4}{3}(\frac{Q^2}{mc^2})^2 c\, \frac{B'^2}{2\mu_0}\, \gamma'^2 = \frac{Z^4}{A^2}\mu^2\, \frac{4}{3}\, c\, \sigma_{\mathrm{T}}\, U'_{B'}\, \gamma'^2 \,, \tag{3}$$

where $E' = mc^2\gamma'$, $\mu \equiv m_{\mathrm{e}}/m_{\mathrm{p}}$, $m = Am_{\mathrm{p}}$ is the mass of an ion with charge Z, σ_{T} is the Thomson cross section, and $U'_{B'}$ is the magnetic energy density. The comoving-frame time $t'_{\mathrm{var}} = \Gamma t_{\mathrm{var}}$, where t_{var} is the variability time in the source frame. The efficiency for a particle to lose its energy through synchrotron losses is $\eta \equiv (t'_{\mathrm{var}}/E')|(\mathrm{d}E'/\mathrm{d}t')_{\mathrm{syn}}|$. Combining the requirement that $\eta > 1$, that is, efficient dissipation of energy via synchrotron losses, and the Hillas condition[20] $E' < Q\,B'R'$, gives a range of allowed energies for which efficient synchrotron radiation is possible, contingent on the strength of the comoving magnetic field B' expressed in Tesla being $\gtrsim 37 \times 10^{-4}\, A^{4/3}Z^{-5/3}(\Gamma/10)^{-2/3}t_4^{-2/3}$, where $t_4 = t_{\mathrm{var}}/(10^4\ \mathrm{s})$. The corresponding energies of escaping cosmic-ray particles (should they be able to escape before losing most of their energy) is $E \cong \Gamma E' \approx 3 \times 10^{20}\, A^{4/3}Z^{-2/3}(\Gamma/10)^{4/3}t_4^{1/3}$ eV. This is the reason proton- and ion-synchrotron models of blazars typically require $B' \gtrsim 10^{-2}$ T, which makes a large demand on jet power, given that equipartition fields (between nonthermal electron and magnetic field) are a few 10^{-4} T. This does not even take into account that the efficient dissipation only applies to the very highest-energy particles. The proton/ion synchrotron radiation is emitted at $E_\gamma^{\mathrm{syn}} \cong 2.0(A^3/Z^2)(\Gamma/10)$ TeV, which for protons is a factor $m_{\mathrm{p}}/m_{\mathrm{e}}$ larger than the well-known leptonic value at $\approx 100\Gamma$ MeV. What is problematic for highly magnetized jets is that for the same synchrotron SED, a larger B' means that the EED peaks at lower comoving Lorentz factors. This not only makes it harder to scatter SSC radiation to TeV energies, but requires that an increasingly large flux of the blazar SED has to have an hadronic origin. See, e.g., [145,146] for proton/ion synchrotron blazar models. Minimizing magnetic power by considering smaller sizes of the emission zone makes that zone more opaque to $\gamma\gamma \rightarrow \mathrm{e}^+ + \mathrm{e}^-$ attenuation, which makes it difficult to explain luminous VHE/TeV radiation from blazars with a proton/ion-synchrotron model.

6.2.2. Photohadronic radiation

Meson production from photohadronic processes in blazar jets is an attractive idea not only because it operates in systems with relativistic particles and large radiation field energy densities, like the blazar environment, but also because it can be established with high confidence by detecting high-energy neutrinos coincident in direction and time with a flaring blazar. The internal synchrotron and direct accretion-disk radiation in blazars is unlikely to be as effective for neutrino production as the external BLR and IR radiation fields [147]. We can simply estimate the photomeson efficiency for jet protons passing through the BLR. Note first that the photohadronic production efficiency of cosmic-ray protons in a blazar jet is hardly distinguishable from the corresponding losses for rectilinear propagation of a cosmic-ray proton through the BLR [148]. Therefore the photohadronic energy-loss rate for a particle of energy $E > E_{\mathrm{thr}}$ is $-(\mathrm{d}E/\mathrm{d}t)_{p\gamma\rightarrow\pi} \cong n_{\mathrm{ph}}\hat{\sigma}Ec$, where $\hat{\sigma} \cong 70$ μb is roughly the product of the photopion cross section and inelasticity above threshold, and n_{ph} is the density of photons. The threshold condition is $(E/m_{\mathrm{p}}c^2)(E_\gamma/m_{\mathrm{e}}c^2) \gtrsim 2m\mu/m_{\mathrm{e}} \cong 300$, so that for Ly α photons dominating the BLR radiation, $E_\gamma/m_{\mathrm{e}}c^2 = 2 \times 10^{-5}$, and $E_{\mathrm{p}} \gtrsim 20$ PeV.

The efficiency to extract proton energy via photomeson processes is $\eta_{p\gamma\rightarrow\pi} = (R/c)|(\mathrm{d}E/\mathrm{d}t)_{p\gamma\rightarrow\pi}|/E$, where $R = 0.1R_{0.1\,\mathrm{pc}}$ pc is the characteristic BLR radius. Using the BLR scaling relation $R_{0.1\,\mathrm{pc}} \sim L_{46}^{1/2}$ (e.g., [149]), where L_{46} is the accretion-disk luminosity in units of 10^{46} erg·s$^{-1} = 10^{39}$ W, then the photon energy density u_{ph} through which the cosmic rays pass is $u_{\mathrm{ph}} \cong L\tau/4\pi R^2 c \cong 3 \times 10^{-3}(\tau/0.1)$ J m^{-3}, where τ is an average covering factor through the BLR. Hence we find that $\eta \cong 3R_{0.1\,\mathrm{pc}}(\tau/0.1)\%$. If ultra-high energy cosmic-ray acceleration takes place in the inner jets of blazars, we can expect ~ 1–10% efficiency [150,148], and a prediction for the neutrino fluxes of blazars given that the baryon loading is normalized by the density of blazars and average power. Note also that Bethe–Heitler photopair losses can provide an injection source of high-energy electrons and positrons, though it is usually less important than photopion production.

Regarding recent progress in hadronic and lepto-hadronic modeling (given that the synchrotron component is widely considered to be nonthermal lepton synchrotron radiation), note that [151] introduces a new lepto-hadronic model. In most cases, leptonic model fits work well, but in flaring sources, implementation of a hadronic component can improve the fits, though at the expense of jet power. In the work of [152], a lepto-hadronic model that includes both lepton and hadron synchrotron and photohadronic processes, operates in the unusual class of HSP BL Lac objects, explaining the weakly VHE variability of the HSP BL Lac objects 1ES 0229+200, 1ES 0347-121 (cf. Fig. 8, upper right), and 1ES 1101-232 as due to the long timescale for hadronic cooling processes. Recent modeling [153] connects the production of PeV neutrinos with the spectral properties of particular blazars that are candidate ultra-high-energy cosmic ray (UHECR) sources.

---

[20] Expressing that the size of the accelerator region should not be smaller than the accelerated particle's Larmor radius.
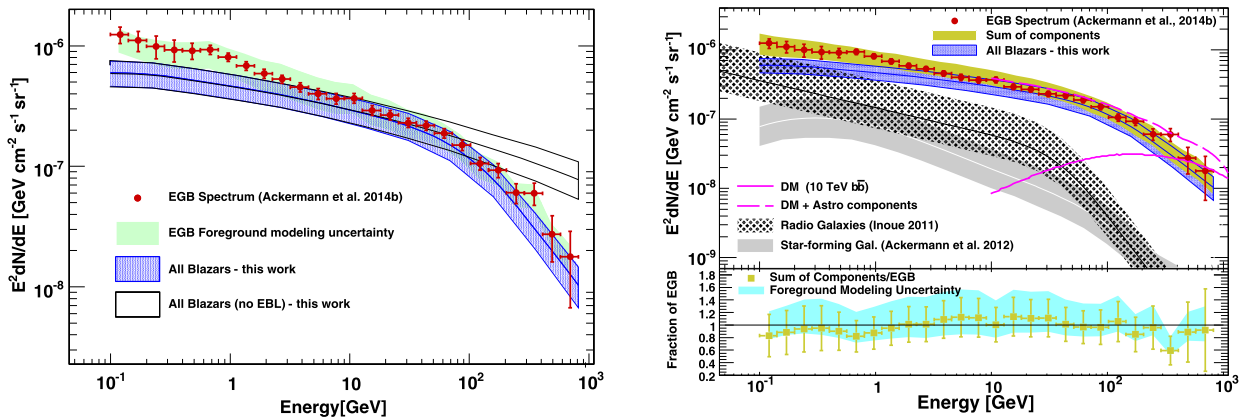
Fig. 14. Contributions of various source classes to the EGB in the analysis of Ajello et al. (2015) [158]. *Left:* Integrated emission of blazars are shown with and without redshift corrections, in comparison with the EGB intensity [2]. *Right:* Decomposition of the EGB intensity into contributions from blazars, radio galaxies, and star-forming galaxies, leaving only a residual intensity from dark matter.

6.3. AGN contribution to the extragalactic γ-ray background

The background γ-ray glow in the intergalactic medium far outside the Milky Way would, according to present understanding, be resolved into scores of blazars and myriad faint radio galaxies and star-forming galaxies that are below present sensitivity. There could be an additional contribution from dark-matter annihilation [154] that would be enhanced in the relaxed environments of old and dwarf elliptical galaxies. Determination of the extragalactic γ-ray background from the Fermi-LAT data requires subtraction of Milky Way point sources and diffuse emission, including the Fermi bubble radiation. What's left over is the extragalactic γ-ray background, including resolved and unresolved extragalactic point sources of radiation, leaving only a weak model dependence from the uncertain quasi-isotropic γ-ray halo formed by cosmic-ray electrons in our Galaxy.

The diffuse isotropic γ-ray background (DIGB), which is the total EGB spectrum including any residual, approximately isotropic, Galactic foregrounds [2], is reported by the Fermi-LAT collaboration to be of the form

$$\epsilon I_\epsilon^{\mathrm{DIGB}} \cong 10^{-2} \left(\frac{E_\gamma}{100\ \mathrm{MeV}}\right)^{-0.32} \exp\left(\frac{-E_\gamma}{280\ \mathrm{GeV}}\right) \frac{\mathrm{GeV}}{\mathrm{m^2 \cdot s \cdot sr}},\ E_\gamma > 0.1\ \mathrm{GeV}. \tag{4}$$

The high-energy cutoff involves, undoubtedly, EBL effects, which is the subject of another paper in this *Comptes rendus* issue [61].

One might imagine that the superposition of countless star-forming galaxies, or radio galaxies, could make up most of the EGB, but in fact they each probably make up $\lesssim 20\%$ each (and their relative contribution is frequency-dependent). A typical L^* (the characteristic luminosity scale of the galaxy luminosity function; see, e.g., [155]) spiral like the Milky Way, with a γ-ray luminosity $L_\gamma \cong 10^{32}\ \mathrm{W} \times L_{39}$ or $10^{39}\ \mathrm{erg \cdot s^{-1}} \times L_{39}$ [156], has a space density of ≈ 1 per 300 Mpc^3, giving an approximate star-forming galaxy γ-ray emissivity $\dot{\varepsilon}_{L^*} \approx 10^{39} L_{39}/300\ \mathrm{Mpc^{-3}}$, implying a γ-ray intensity from L^* galaxies $I_{L^*} \approx R_\mathrm{H} \dot{\varepsilon}_{L^*}/4\pi \cong 8 \times 10^{-8} \zeta_z L_{39}\ \mathrm{GeV\,cm^{-2} \cdot s^{-1} \cdot sr^{-1}}$). The factor $\zeta_z \approx 2$–3 accounts for increased star formation rate at $z \gtrsim 1$. Taking into account a bolometric factor implies that the γ-ray intensity from star-forming galaxies is at the 10–20% level of the total EGB or DIGB intensity in Eq. (4). The cores of radio galaxies and radio galaxy emissions [157] probably make up another sub-dominant but non-negligible fraction of the EGB.

The contribution of BL Lac objects [35] and FSRQs [159] to the EGB is achieved quantitatively by constructing the evolving luminosity distribution of the two source populations. A recent decomposition of the EGB based upon luminosity function of bright Fermi-LAT γ-ray blazars [158] finds that $\approx 50\%$ of the total EGB is resolved into blazars, but only $\lesssim 20\%$ of the remainder can originate from blazars (Fig. 14). Using models for the radio galaxy and star-forming populations leaves the maximum contribution from other sources, including dark matter. This technique provides one of the strongest constraints on dark matter cross sections. See also Ref. [160].

7. Conclusions: γ-ray AGN

The HE and VHE γ-ray sky has undergone a sea change in the last decade, thanks primarily to the Fermi Gamma ray Space Telescope in space and new arrays of IACTs on the ground, including the 4×13 m VERITAS array, the 2×17 m MAGIC telescopes, and the 4×13 m H.E.S.S.–I array which, with the addition of the big 28 m telescope, makes the H.E.S.S.–II. The High Altitude Water Cherenkov (HAWC) observatory, the successor to the Milagro all-sky TeV telescope, is now inaugurated and taking data with its full complement of 300 tanks.

At the same time, only limited advances have been made on AGN science in the MeV regime. Above 1 MeV, INTEGRAL has not been more sensitive than COMPTEL on CGRO, and only a small fraction of its time was spent off the Galactic plane
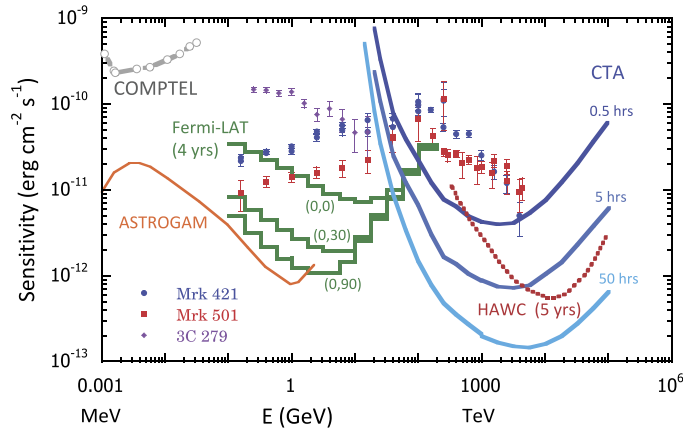
Fig. 15. Sensitivity of γ-ray observatories. Nominal CTA sensitivity requirements for exposures of 0.5 h, 5 h, and 50 h, as labeled [161]. The field of view of CTA is a few degrees wide. The HAWC sensitivity is for 5 yrs of exposure [162]. The Fermi-LAT differential sensitivity plot [163] is for four years, in 4 bins per energy decade, at Galactic longitude ℓ and latitude b of $(\ell, b) = (0, 0), (0, 30)$, and $(0, 90)$, as labeled, that is, at the Galactic center, intermediate latitudes, and at the north Galactic pole, respectively. The sensitivity uses Pass 7 Fermi-LAT instrument response to detect a point source of γ rays with a -2 power-law photon number spectrum, and >10 photons per energy band. The Pass 8 instrument responses made available recently might change these estimations. The COMPTEL sensitivity is for the entire CGRO mission from 1991 to 2000 [164]. The ASTROGAM sensitivity is for three years in the scanning mode at high Galactic latitude [162].

looking at extragalactic AGN. The "MeV blindness" ends below ∼100 keV with IBIS on INTEGRAL, with the Swift-BAT surveys, hard X-ray spectroscopy of sources with NuSTAR, and the upcoming ASTRO-H, while the Fermi-LAT pair-production tracker design becomes most sensitive well above ∼100 MeV. At the present moment, there is no consensus and few designs for a successor to Fermi-LAT in the ≈0.1–100 GeV range.

The next big activity in γ-ray astronomy is, of course, the Cherenkov Telescope Array (CTA), with its siting in both the Northern and Southern Hemispheres recently announced. CTA, and other proposed γ-ray activities, are discussed elsewhere in this volume [162]. With regard to γ-ray AGN specifically, Fig. 15 shows Fermi-LAT, CTA, and HAWC sensitivity curves, in comparison with νF_ν SEDs of Mrk 421, Mrk 501, and 3C 279 (data from the same epochs as in Fig. 10). The sensitivity curves are relative to SEDs, thus to differential photon fluxes multiplied by E^2, so the data comparison should be made with care, not to mention the differences in exposure and field of view in the different curves, as described in the caption to Fig. 15. The sensitivity graph of ASTROGAM [162], recently proposed for an ESA M4 opportunity, is also shown in Fig. 15.

One thing that will surely hamper blazar studies in the future is the lack of spectral definition in the ∼0.2–100 MeV range, where separate IR radiation fields deep in the black hole are exposed through their Compton signatures. This is the regime of the hypothetical "extreme" blazar, whose νF_ν peak synchrotron frequency is at MeV energies. This is where the νF_ν γ-ray Compton peaks of LSP blazars are found, and where the SSC emission component gives way to the EC component when there is an external radiation field. This is where, if blazars share any similarity with γ-ray bursts [165], a quasi-thermal photosphere from the blazar engine could be detected.

7.1. GeV–TeV connection

The combination of Fermi-LAT and the current generation of IACTs allows for unprecedented γ-ray coverage, with the high-energy component of blazar SEDs sampled with hitherto unmatched resolution, permitting a much improved characterization of the peak emission and γ-ray spectrum [166]. Given the slight overlap in energy with ground-based detectors, Fermi-LAT, with its wide field of view, has increased the efficiency of catching VHE emission of flaring blazars with IACTs. The higher accuracy of spectral measurements in both HE and VHE has improved the search for direct evidence of EBL-induced spectral steepening in GeV–TeV blazars, since the HE and VHE spectral photon indices for a sample of GeV–TeV blazars show a clear correlation with redshift [167]. The size of the spectral break is in all cases compatible or larger than the one expected from HE–VHE γ rays interacting with the EBL, which can sometimes mean that the *intrinsic* SED is not peaking where the *observed* SED peaks.

Fermi-LAT continues to work hand in glove with the IACTs and water Cherenkov detectors. The population explosion of VHE sources shown in Fig. 3 right was, after 2008, in significant part due to the Fermi-LAT detection of hard, ≳100 GeV photons from high-latitude sources. The sky at ≳10 GeV, as reported in the First Fermi-LAT Hard Source Catalog (1FHL) [168], contains 514 objects, of which ∼75% are BL Lac objects. The Second Catalog of hard Fermi-LAT sources (2FHL) at >50 GeV [169] based on Pass 8 analysis comprises ∼350 sources over the full sky, of which ∼145 are found in the VHE catalog. Above 10 GeV, the Fermi bubbles stand out above the background in the Fermi-LAT sky maps, but are difficult to see with IACTs because of their extension. With a systematic VHE survey, statistical studies comparing VHE γ-ray spectral indices with luminosity and peak frequencies, such as those found with Fermi-LAT, will be possible. HAWC will provide the best large field of view γ-ray sky maps above ≈1 TeV, and will be sensitive to day-scale flaring of the brightest BL Lac objects.

7.2. Whither γ-ray AGN astronomy?

Now that the Fermi Gamma ray Space Telescope has begun its 8th year of operations, and the VERITAS, MAGIC, and H.E.S.S. IACT arrays are, within ≈ 5 yrs, to be overshadowed by CTA, we may ask "whither γ-ray astronomy of AGN?" that is, where are we headed? The important thing is that technology is evolving, even when the observatories go dark. The extraordinarily dynamic SEDs of γ-ray AGN now measured with ground-based and space-based facilities reveal the nature of the extreme black-hole jet environment, and tell us how black holes accumulate mass and dissipate energy. In statistical samples, they tell us how blazars and radio galaxies evolve over cosmic time. Both observationally and theoretically, major advances have been made in measuring and deciphering the SEDs of γ-ray emitting blazars in the quarter century since the γ-ray blazar class was discovered. Some of the big puzzles that γ-ray AGN astronomy can address and solve are: What powers the jets of supermassive black holes? What causes the variability time scale to be so short during intense flaring periods? Do shocks or turbulence in blazar jets accelerate the ultra-high energy cosmic rays [170], or do UHECRs have a different origin? What acceleration and radiation physics explains the peak synchrotron and Compton frequencies of blazars of different types? How much can we limit the dark-matter cross section by modeling the γ-ray background light?

In the last decade, the number of γ-ray emitting AGN has increased by more than an order of magnitude, and new classes of extragalactic γ-ray emitters have emerged in both the HE and VHE regimes. The better sensitivity of these observatories has also improved our knowledge of the time-dependent behavior of AGN, further pushing the need for dynamical radiative modeling, which are more complex than static models but allow details about the acceleration mechanisms to be modeled. The AGN paradigm receives new challenges, for example, the inability of simple kinematic shell models to explain rapid variability, which may be achieved through magnetic reconnection; breakdown of one-zone models; extremely hard spectra of flaring events in FSRQs; identification of robust correlations in statistical samples of blazars, etc. The advent of the next generation of ground-based γ-ray telescopes, namely HAWC and CTA, will open up the γ-ray sky and provide data to answer important questions in high-energy astronomy and particle astrophysics, but the lack of a sensitive MeV-regime space telescope will impede a deeper understanding of γ-ray AGN and, indeed, the high-energy sky.

Acknowledgements

References

[1] S. Ohm, C. R. Physique 17 (6) (2016) 585–593, this issue.
[2] M. Ackermann, M. Ajello, A. Albert, et al., Astrophys. J. 799 (2015) 86.
[3] C.D. Dermer, N. Gehrels, Astrophys. J. 447 (1995) 103.
[4] C.M. Urry, P. Padovani, Publ. Astron. Soc. Pac. 107 (1995) 803.
[5] B.L. Fanaroff, J.M. Riley, Mon. Not. R. Astron. Soc. 167 (1974) 31P.
[6] P. Giommi, P. Padovani, G. Polenta, et al., Mon. Not. R. Astron. Soc. 420 (2012) 2899.
[7] J. Biteau, PhD thesis, 2013, pastel-00822242, version 1.
[8] B. Degrange, G. Fontaine, C. R. Physique 16 (2015) 587.
[9] B.N. Swanenburg, et al., Nature 275 (1978) 298.
[10] D.J. Thomson, C. R. Physique 16 (2015) 600.
[11] L. Bassani, A.J. Dean, Space Sci. Rev. 35 (1983) 367.
[12] C.D. Dermer, R. Schlickeiser, A. Mastichiadis, Astron. Astrophys. 256 (1992) L27.
[13] R.C. Hartman, et al., Astrophys. J. Suppl. Ser. 123 (1999) 79.
[14] M. de Naurois, D. Mazin, C. R. Physique 16 (2015) 610.
[15] T.C. Weekes, M.F. Cawley, D.J. Fegan, et al., Astrophys. J. 342 (1989) 379.
[16] M. Punch, C.W. Akerlof, M.F. Cawley, et al., Nature 358 (1992) 477.
[17] C.E. Fichtel, D.L. Bertsch, J. Chiang, et al., Astrophys. J. Suppl. Ser. 94 (1994) 551.
[18] D.J. Thompson, D.L. Bertsch, B.L. Dingus, et al., Astrophys. J. Suppl. Ser. 101 (1995) 259.
[19] A.A. Abdo, M. Ackermann, M. Ajello, et al., Astrophys. J. 700 (2009) 597.
[20] A.A. Abdo, M. Ackermann, M. Ajello, et al., Astrophys. J. 715 (2010) 429.
[21] M. Ackermann, et al., Astrophys. J. 743 (2011) 171;
     M. Ackermann, et al., (e) Astrophys. J. 806 (2015) 144.
[22] M. Ackermann, M. Ajello, W. Atwood, et al., Astrophys. J. 810 (2015) 14.
[23] C.D. Dermer, G. Menon, High Energy Radiation from Black Holes, Princeton Series in Astrophysics, 2009.
[24] S.C. Unwin, M.H. Cohen, J.A. Biretta, et al., Astrophys. J. 289 (1985) 109.
[25] A. Königl, Astrophys. J. 243 (1981) 700.
[26] M.C. Begelman, R.D. Blandford, M.J. Rees, Rev. Mod. Phys. 56 (1984) 255.
[27] P. Sreekumar, D.L. Bertsch, B.L. Dingus, et al., Astrophys. J. Lett. 400 (1992) L67.
[28] A.A. Abdo, M. Ackermann, M. Ajello, et al., Astron. Astrophys. 523 (2010) AA46.
[29] A.A. Abdo, M. Ackermann, M. Ajello, et al., Astrophys. J. Lett. 709 (2010) L152.
[30] F. Acero, F. Aharonian, A.G. Akhperjanian, et al., Science 326 (2009) 1080.
[31] VERITAS Collaboration, V.A. Acciari, E. Aliu, et al., Nature 462 (2009) 770.
[32] M. Su, C. van Eldik, C. R. Physique 16 (2015) 686.

[33] D.A. Sanchez, F. Brun, C. Couturier, A. Jacholkowska, J.-P. Lenain, in: The Fourth Fermi Symposium, 2015.
[34] M.S. Shaw, R.W. Romani, G. Cotter, et al., Astrophys. J. 764 (2013) 135.
[35] M. Ajello, et al., Astrophys. J. 780 (2014) 73.
[36] A.A. Abdo, M. Ackermann, M. Ajello, et al., Astrophys. J. Lett. 733 (2011) LL26.
[37] A.A. Abdo, et al., Astrophys. J. 720 (2010) 912.
[38] A.P. Marscher, W.K. Gear, Astrophys. J. 298 (1985) 114.
[39] L. Fuhrmann, S. Larsson, J. Chiang, et al., Mon. Not. R. Astron. Soc. 441 (2014) 1899.
[40] A.A. Abdo, M. Ackermann, M. Ajello, et al., Science 328 (2010) 725.
[41] A.A. Abdo, M. Ackermann, M. Ajello, et al., Astrophys. J. 720 (2010) 912.
[42] M.L. Lister, D.C. Homan, Astron. J. 130 (2005) 1389.
[43] M. Kadler, D. Eisenacher, E. Ros, et al., Astron. Astrophys. 538 (2012) L1.
[44] J. Aleksić, L.A. Antonelli, P. Antoranz, et al., Astrophys. J. Lett. 723 (2010) L207.
[45] A. Neronov, D. Semikoz, I. Vovk, Astron. Astrophys. 519 (2010) LL6.
[46] M. Georganopoulos, R.M. Sambruna, D. Kazanas, et al., Astrophys. J. Lett. 686 (2008) L5.
[47] G. Migliori, P. Grandi, E. Torresi, et al., Astron. Astrophys. 533 (2011) AA72.
[48] A.A. Abdo, et al., Astrophys. J. Lett. 707 (2009) L142.
[49] R.W. Pogge, New Astron. Rev. 44 (2000) 381.
[50] M. Böttcher, C. Dermer, Astrophys. J. 564 (2002) 86.
[51] P.N. Werner, D.M. Worrall, M. Birkinshaw, in: Particles and Fields in Radio Galaxies Conference, 2001, pp. 250–294.
[52] http://www.werner.lu/pn/phd/ngc6251.html.
[53] F. Aharonian, et al., Astron. Astrophys. 403 (2003) 1.
[54] F. Acero, et al., Astrophys. J. Suppl. Ser. 218 (2015) 23.
[55] A. Abramowski, et al., Astrophys. J. 2 (2012) 746.
[56] J. Aleksić, et al., Science 346, 1080.
[57] Ł. Stawarz, L. Ostorero, M.C. Begelman, et al., Astrophys. J. 680 (2008) 911.
[58] C. Müller, M. Kadler, R. Ojha, et al., Astron. Astrophys. 562 (2014) A4.
[59] M. Ackermann, M. Ajello, A. Allafort, et al., Astrophys. J. 747 (2012) 104.
[60] R.D. Blandford, H. Netzer, L. Woltjer, in: T.J.-L. Courvoisier, M. Mayor (Eds.), Active Galactic Nuclei, in: Saas-Fee Advanced Courses, 1990.
[61] D. Horns, A. Jacholkowska, C. R. Physique 17 (6) (2016) 632–648, this issue.
[62] A.A. Abdo, M. Ackermann, M. Ajello, et al., Nature 463 (2010) 919.
[63] A.A. Abdo, et al., Astrophys. J. 727 (2011) 129.
[64] A.A. Abdo, M. Ackermann, M. Ajello, et al., Astrophys. J. 707 (2009) 55.
[65] A.A. Abdo, M. Ackermann, M. Ajello, et al., Astrophys. J. 699 (2009) 31.
[66] G. Henri, L. Saugé, Astrophys. J. 640 (2006) 185.
[67] G. Ghisellini, F. Tavecchio, M. Chiaberge, Astron. Astrophys. 432 (2005) 401.
[68] M. Georganopoulos, D. Kazanas, Astrophys. J. Lett. 594 (2003) L27.
[69] I.I.K. Pauliny-Toth, K.I. Kellermann, Astrophys. J. 146 (1966) 634.
[70] T.W. Jones, G.R. Burbidge, Astrophys. J. 186 (1973) 791.
[71] D.A. Kniffen, D.L. Bertsch, C.E. Fichtel, et al., Astrophys. J. 411 (1993) 133.
[72] A.A. Abdo, M. Ackermann, M. Ajello, et al., Astrophys. J. 733 (2011) LL26.
[73] Y.T. Tanaka, Ł. Stawarz, D.J. Thompson, et al., Astrophys. J. 733 (2011) 19.
[74] S. Saito, Ł. Stawarz, Y.T. Tanaka, et al., Astrophys. J. 766 (2013) LL11.
[75] A.M. Brown, Mon. Not. R. Astron. Soc. 431 (2013) 824.
[76] L. Foschini, G. Ghisellini, F. Tavecchio, G. Bonnoli, A. Stamerra, Astron. Astrophys. 530 (2011) AA77.
[77] K. Nalewajko, Mon. Not. R. Astron. Soc. 430 (2013) 1324.
[78] B. Lott, in: Assessing the Short-Timescale Variability in LAT Blazars, Fermi Symposium, Nagoya, Japan, 2014.
[79] L. Ferrarese, D. Merritt, Astrophys. J. 539 (2000) 9.
[80] C.M. Urry, R. Scarpa, M. O'Dowd, et al., Astrophys. J. 532 (2000) 816.
[81] D.J. Macomb, C.W. Akerlof, H.D. Aller, et al., Astrophys. J. 449 (1995) L99.
[82] F.A. Aharonian, et al., Astrophys. J. 664 (2007) L71.
[83] J. Albert, E. Aliu, H. Anderhub, et al., Astrophys. J. 669 (2007) 862.
[84] L. Fortson, Fermi-LAT Collaborators, VERITAS Collaboration, American Institute of Physics Conference Series, vol. 1505, 2012, p. 514.
[85] H.E.S.S. Collaboration, A. Abramowski, F. Acero, et al., Astron. Astrophys. 539 (2012) A149.
[86] F.A. Aharonian, et al., Astron. Astrophys. 473 (2007) 25.
[87] M.C. Begelman, A.C. Fabian, M.J. Rees, Mon. Not. R. Astron. Soc. 384 (2008) L19.
[88] M. Cerruti, for the VERITAS Collaboration, arXiv:1307.8091, 2013.
[89] J. Aleksić, L.A. Antonelli, P. Antoranz, et al., Astrophys. J. 730 (2011) LL8.
[90] MAGIC Collaboration, J. Albert, E. Aliu, et al., Science 320 (2008) 1752.
[91] J. Aleksić, L.A. Antonelli, P. Antoranz, et al., Astron. Astrophys. 530 (2011) AA4.
[92] S. Vercellone, A.W. Chen, A. Giuliani, et al., Astrophys. J. 676 (2008) L13.
[93] A.A. Abdo, M. Ackermann, M. Ajello, et al., Astrophys. J. 699 (2009) 817.
[94] A.A. Abdo, M. Ackermann, M. Ajello, et al., Astrophys. J. 710 (2010) 1271.
[95] M. Ackermann, M. Ajello, L. Baldini, et al., Astrophys. J. 721 (2010) 1383.
[96] J.R. Mattox, S.J. Wagner, M. Malkan, et al., Astrophys. J. 476 (1997) 692.
[97] A.A. Abdo, M. Ackermann, M. Ajello, et al., Astrophys. J. 722 (2010) 520.
[98] J. Poutanen, B. Stern, Astrophys. J. 717 (2010) L118.
[99] B.E. Stern, J. Poutanen, Mon. Not. R. Astron. Soc. 417 (2011) L11.
[100] M. Cerruti, C.D. Dermer, B. Lott, C. Boisson, A. Zech, Astrophys. J. 771 (2013) LL4.
[101] C.D. Dermer, M. Cerruti, B. Lott, C. Boisson, A. Zech, Astrophys. J. 782 (2014) 82.
[102] M. Błażejowski, M. Sikora, R. Moderski, G.M. Madejski, Astrophys. J. 545 (2000) 107.
[103] A.P. Marscher, S.G. Jorstad, F.D. D'Arcangelo, et al., Nature 452 (2008) 966.
[104] A.P. Marscher, S.G. Jorstad, V.M. Larionov, et al., Astrophys. J. 710 (2010) L126.
[105] I. Agudo, S.G. Jorstad, A.P. Marscher, et al., Astrophys. J. 726 (2011) LL13.
[106] I. Agudo, A.P. Marscher, S.G. Jorstad, et al., arXiv:1303.2039, 2013.

[107] A.B. Pushkarev, Y.Y. Kovalev, M.L. Lister, Astrophys. J. 722 (2010) L7.
[108] J.L. Richards, W. Max-Moerbeck, V. Pavlidou, et al., Astrophys. J. Suppl. Ser. 194 (2011) 29.
[109] J.D. Finke, C.D. Dermer, Astrophys. J. 714 (2010) L303.
[110] L. Pacciani, F. Tavecchio, I. Donnarumma, et al., Astrophys. J. 790 (2014) 45.
[111] M. Hayashida, K. Nalewajko, G.M. Madejski, et al., arXiv:1502.04699, 2015.
[112] K. Nalewajko, M.C. Begelman, B. Cerutti, D.A. Uzdensky, M. Sikora, Mon. Not. R. Astron. Soc. 425 (2012) 2519.
[113] M. Ackermann, M. Ajello, A. Albert, et al., Astrophys. J. 771 (2013) 57.
[114] H. Anderhub, M. Backes, A. Biland, et al., J. Instrum. 8 (2013) P06008.
[115] G. Fossati, et al., Mon. Not. R. Astron. Soc. 299 (1998) 433.
[116] E.T. Meyer, G. Fossati, M. Georganopoulos, M.L. Lister, Astrophys. J. 740 (2011) 98.
[117] F. Aharonian, et al., Astrophys. J. 696 (2009) 150.
[118] M. Hayashida, G.M. Madejski, K. Nalewajko, et al., Astrophys. J. 754 (2012) 114.
[119] K.R. Lind, R.D. Blandford, Astrophys. J. 295 (1985) 358.
[120] G. Ghisellini, et al., Mon. Not. R. Astron. Soc. 301 (1998) 451.
[121] J. Finke, Astrophys. J. 763 (2013) 134.
[122] G. Ghisellini, L. Maraschi, F. Tavecchio, Mon. Not. R. Astron. Soc. 396 (2009) 10.
[123] G. Ghisellini, F. Tavecchio, L. Foschini, G. Ghirlanda, Mon. Not. R. Astron. Soc. 414 (2011) 2674.
[124] G. Ghisellini, F. Tavecchio, L. Foschini, et al., Mon. Not. R. Astron. Soc. 402 (2010) 497.
[125] G. Nandikotkur, et al., Astrophys. J. 657 (2007) 706.
[126] A.A. Abdo, M. Ackermann, I. Agudo, et al., Astrophys. J. 716 (2010) 30.
[127] C.D. Dermer, D. Yan, L. Zhang, J.D. Finke, B. Lott, Astrophys. J. 809 (2015) 174.
[128] E. Massaro, M. Perri, P. Giommi, R. Nesci, F. Verrecchia, Astron. Astrophys. 422 (2004) 103.
[129] M. Malkov, L. O'C Drury, Rep. Prog. Phys. 64 (2000) 429.
[130] C.D. Dermer, Mem. Soc. Astron. Ital. 86 (2015) 13.
[131] M. Böttcher, D.E. Harris, H. Krawczynski, Relativistic Jets from Active Galactic Nuclei, Wiley, Berlin, 2012.
[132] A.A. Abdo, et al., Astrophys. J. 736 (2011) 131.
[133] D. Giannios, D.A. Uzdensky, M.C. Begelman, Mon. Not. R. Astron. Soc. 402 (2010) 1649.
[134] A.P. Marscher, S.G. Jorstad, arXiv:1005.5551, 2010.
[135] R. Narayan, T. Piran, Mon. Not. R. Astron. Soc. 420 (2012) 604.
[136] A.P. Marscher, S.G. Jorstad, I. Agudo, N.R. MacDonald, T.L. Scott, arXiv:1204.6707, 2012.
[137] K. Nalewajko, M.C. Begelman, B. Cerutti, D.A. Uzdensky, M. Sikora, Mon. Not. R. Astron. Soc. 425 (2012) 2519.
[138] P. Subramanian, A. Shukla, P.A. Becker, Mon. Not. R. Astron. Soc. 423 (2012) 1707.
[139] H. Krawczynski, S.B. Hughes, D. Horan, et al., Astrophys. J. 601 (2004) 151.
[140] M. Böttcher, Astrophys. J. 621 (2005) 176.
[141] W. Essey, A. Kusenko, Astropart. Phys. 33 (2010) 81.
[142] W. Essey, O.E. Kalashev, A. Kusenko, J.F. Beacom, Phys. Rev. Lett. 104 (2010) 141102.
[143] M.G. Aartsen, M. Ackermann, J. Adams, et al., Phys. Rev. Lett. 113 (2014) 101101.
[144] F. Krauß, M. Kadler, K. Mannheim, et al., Astron. Astrophys. 566 (2014) L7.
[145] F.A. Aharonian, Mon. Not. R. Astron. Soc. 332 (2002) 215.
[146] A. Mücke, R.J. Protheroe, R. Engel, J.P. Rachen, T. Stanev, Astropart. Phys. 18 (2003) 593.
[147] A. Atoyan, C.D. Dermer, Phys. Rev. Lett. 87 (2001) 221102.
[148] C.D. Dermer, K. Murase, Y. Inoue, J. High Energy Astrophys. 3 (2014) 29.
[149] G. Ghisellini, F. Tavecchio, Mon. Not. R. Astron. Soc. 387 (2008) 1669.
[150] K. Murase, Y. Inoue, C.D. Dermer, Phys. Rev. D 90 (2014) 023007.
[151] M. Böttcher, A. Reimer, K. Sweeney, A. Prakash, Astrophys. J. 768 (2013) 54.
[152] M. Cerruti, A. Zech, C. Boisson, S. Inoue, Mon. Not. R. Astron. Soc. 448 (2015) 910.
[153] M. Petropoulou, S. Dimitrakoudis, P. Padovani, A. Mastichiadis, E. Resconi, Mon. Not. R. Astron. Soc. 448 (2015) 2412.
[154] P. Brun, J. Cohen-Tanugi, C. R. Physique 17 (6) (2016) 649–662, this issue.
[155] A. Cooray, M. Milosavljević, Astrophys. J. 627 (2005) 89.
[156] A.W. Strong, T.A. Porter, S.W. Digel, et al., Astrophys. J. 722 (2010) L58.
[157] Y. Inoue, Astrophys. J. 733 (2011) 66.
[158] M. Ajello, D. Gasparrini, M. Sánchez-Conde, et al., Astrophys. J. 800 (2015) LL27.
[159] M. Ajello, M.S. Shaw, R.W. Romani, et al., Astrophys. J. 751 (2012) 108.
[160] F.W. Stecker, T.M. Venters, Astrophys. J. 736 (2011) 40.
[161] M. Actis, G. Agnetta, A. Akhperjanian, et al., Exp. Astron. 32 (2011) 193.
[162] J. Knödlseder, C. R. Physique 17 (6) (2016) 663–678, this issue.
[163] Fermi-LAT performance at http://www.slac.stanford.edu/exp/glast/groups/canda/lat_Performance.htm.
[164] V. Schönfelder, New Astron. Rev. 48 (2004) 193.
[165] F. Piron, C. R. Physique 17 (6) (2016) 617–631, this issue.
[166] G.D. Sentürk, et al., Astrophys. J. 764 (2013) 119.
[167] D. Sanchez, S. Fegan, B. Giebels, Astron. Astrophys. 554 (2013) 75.
[168] M. Ackermann, M. Ajello, A. Allafort, et al., Astrophys. J. Suppl. Ser. 209 (2013) 34.
[169] M. Ackermann, M. Ajello, W.B. Atwood, et al., Astrophys. J. Suppl. 222 (2016) 5.
[170] A. Letessier-Selvon (Ed.), Ultra-high-energy cosmic rays: from the ankle to the tip of the spectrum, C. R. Physique 15 (4) (2014) 297–384.